

Metadata of the chapter that will be visualized online

Chapter Title	Remote Sensing of Ocean Color	
Copyright Year	2011	
Copyright Holder	Springer Science+Business Media, LLC	
Corresponding Author	Family Name	Dierssen
	Particle	
	Given Name	Heidi
	Suffix	
	Division/Department	Department of Marine Sciences/Geography
	Organization/University	University of Connecticut
	City	Groton
	State	CT
	Postcode	06340
	Country	USA
	Email	heidi.dierssen@uconn.edu
Author	Family Name	Randolph
	Particle	
	Given Name	Kaylan
	Suffix	
	Division/Department	Department of Marine Sciences/Geography
	Organization/University	University of Connecticut
	City	Groton
	State	CT
	Postcode	06340
	Country	USA
Abstract	<p>The oceans cover over 70% of the earth's surface and the life inhabiting the oceans play an important role in shaping the earth's climate. Phytoplankton, the microscopic organisms in the surface ocean, are responsible for half of the photosynthesis on the planet. These organisms at the base of the food web take up light and carbon dioxide and fix carbon into biological structures releasing oxygen. Estimating the amount of microscopic phytoplankton and their associated primary productivity over the vast expanses of the ocean is extremely challenging from ships. However, as phytoplankton take up light for photosynthesis, they change the color of the surface ocean from blue to green. Such shifts in ocean color can be measured from sensors placed high above the sea on satellites or aircraft and is called "ocean color remote sensing." In open ocean waters, the ocean color is predominantly driven by the phytoplankton concentration and ocean color remote sensing has been used to estimate the amount of chlorophyll <i>a</i>, the primary light-absorbing pigment in all phytoplankton. For the last few decades, satellite data have been used to estimate large-scale patterns of chlorophyll and to model primary</p>	

productivity across the global ocean from daily to interannual timescales. Such global estimates of chlorophyll and primary productivity have been integrated into climate models and illustrate the important feedbacks between ocean life and global climate processes. In coastal and estuarine systems, ocean color is significantly influenced by other light-absorbing and light-scattering components besides phytoplankton. New approaches have been developed to evaluate the ocean color in relationship to colored dissolved organic matter, suspended sediments, and even to characterize the bathymetry and composition of the seafloor in optically shallow waters. Ocean color measurements are increasingly being used for environmental monitoring of harmful algal blooms, critical coastal habitats (e.g., seagrasses, kelps), eutrophication processes, oil spills, and a variety of hazards facing the coastal zone.

R

1

2 Remote Sensing of Ocean Color

3 HEIDI DIERSSEN, KAYLAN RANDOLPH
4 University of Connecticut
5 Groton, CT, USA

Au1 6 Article Outline

7 Glossary
8 Definition of the Subject, Relevance, Motivation
9 Introduction
10 Optical Properties of the Water Column
11 Basics of Ocean Color Remote Sensing
12 Ocean Color Algorithms
13 Applications for Oceanography
14 Applications for Environmental Monitoring
15 Future Directions
16 Bibliography

17 Glossary

18 **Absorption, $a(\lambda)$** The fraction of a collimated beam of
19 photons in a particular wavelength (λ), which is
20 absorbed or scattered per unit distance within the
21 medium (units 1/length or m^{-1}). Photons which
22 are absorbed by ocean water alter the spectral dis-
23 tribution of light that can be observed remotely.

24 **Apparent optical properties (AOP)** Optical proper-
25 ties which depend primarily on the medium itself
26 but have a small dependence on the ambient light
27 field. Typically, AOPs are derived from measure-
28 ments of the ambient light field, particularly
29 upwelling and downwelling radiance and irradi-
30 ance. Principal AOPs include irradiance reflectance,
31 remote sensing reflectance, and the diffuse attenu-
32 ation coefficients.

33 **Backscattering, $b_b(\lambda)$** Light of a particular wavelength
34 (λ) that is scattered in a direction $90\text{--}180^\circ$ away
35 from its original path (i.e., backward hemisphere).

Backscattered light is what is measured as ocean 36
color in remote sensing, namely, downward propa- 37
gating sunlight that has been redirected back 38
toward the sea surface and out into the atmosphere. 39
For natural waters, only a few percent of the light 40
entering the ocean is backscattered out. 41

Colored or chromophoric dissolved organic material 42
(CDOM) CDOM is yellow-brown in color and 43
absorbs primarily ultraviolet and blue light decreas- 44
ing exponentially with increasing wavelength. Pro- 45
duced from the decay of plant material, it consists 46
mainly of humic and fulvic acids and is operation- 47
ally defined as substances that pass through a $0.2\ \mu\text{m}$ 48
filter. 49

Diffraction Light which propagates or bends along 50
the boundary of two different mediums with dif- 51
ferent indices of refraction. 52

Diffuse attenuation coefficient, $K(\lambda)$ A normalized 53
depth derivative that describes the change of light, 54
plane incident irradiance, with depth. The rate of 55
diminution of sunlight with depth underwater is 56
typically logarithmic. 57

Index of refraction (real), n The speed of light in 58
a medium, c_{med} , relative to the speed of light in 59
a vacuum, c_v , expressed as $n = c_v/c_{med}$. The real 60
index of refraction determines the scattering of 61
light at the boundary between two different 62
mediums and within the medium from thermal 63
and molecular fluctuations. The relative refractive 64
index, n' , is the ratio of the speed of light within the 65
medium, c_m , to the speed of light within a particle, 66
 c_p . As n' deviates from 1, the scattering caused by 67
the particle increases for a general size and shape 68
particle (e.g., minerals and microbubbles). 69

Inherent optical properties (IOP) Optical properties 70
which depend on the medium itself and are inde- 71
pendent of the ambient light field. IOPs are defined 72
from a parallel beam of light incident on a thin layer 73
of the medium. Two fundamental IOPs are the 74
absorption (a) and the volume scattering 75

76 coefficient (β), which describe how light is either
 77 absorbed or directionally scattered by ocean water.

78 **Irradiance (downward planar), $E_d(\lambda)$** The incremen-
 79 tal amount of radiant energy per unit time (W)
 80 incident on the sensor area (m^{-2}) from all solid
 81 angles contained in the upper hemisphere,
 82 expressed per unit wavelength of light (λ , nm^{-1}).
 83 This is used to measure the amount of spectral
 84 energy from the sun reaching the sea surface.

85 **Irradiance reflectance, $R(\lambda)$** The ratio of the upwell-
 86 ing irradiance, $E_u(\lambda)$, to the plane downwelling
 87 irradiance, $E_d(\lambda)$, in different wavelengths (λ).

88 **Optical depth, ζ** A measure of how opaque a medium
 89 is to radiation. The optical depth is a function of the
 90 geometric depth and the vertical attenuation
 91 coefficient.

92 **Optically shallow waters** An aquatic system where the
 93 spectral reflectance off the bottom contributes to
 94 radiance measured above the sea surface and is
 95 defined by the water clarity, bottom depth, and
 96 bottom composition.

97 **Photosynthetically available radiation (PAR)** The
 98 integrated photon flux (photons per second per
 99 square meter) within the 400–700 nm wavelength
 100 range at the ocean surface. PAR is the total energy
 101 available to phytoplankton for photosynthesis and
 102 is reported in units of $Q\ m^{-2}\ s^{-1}$, where Q is
 103 quanta, or in $\mu E\ m^{-2}\ s^{-1}$, where E is Einsteins.

104 **Radiance, $L(\lambda)$** The incremental amount of radiant
 105 energy per unit time (in Watts) incident on the
 106 sensor area (m^{-2}) in a solid angle view (sr^{-1}) per
 107 unit wavelength (λ) of light (nm^{-1}). A satellite
 108 measures radiance.

109 **Reflection** At the boundary of two different mediums
 110 with different indices of refraction, a certain
 111 amount of radiation is returned at an angle equal
 112 to the angle of incidence.

113 **Refraction** The direction of light propagation
 114 changes, or is bent, at the boundary between two
 115 mediums with different indices of refraction. The
 116 refracted light bends toward the normal boundary
 117 when the index of refraction increases from one
 118 medium to another and away from the normal
 119 boundary when the index of refraction decreases
 120 from one medium to another.

121 **Remote sensing reflectance, $R_{rs}(\lambda)$** A specialized ratio
 122 used for remote sensing purposes formulated as the

ratio of the spectral water-leaving radiance, $L_w(\lambda)$, 123
 to the plane irradiance incident on the water, $E_d(\lambda)$. 124
 It represents the spectral distribution of sunlight 125
 penetrating the sea surface that is backscattered 126
 out again and potentially measured remotely. The- 127
 oretically, it is proportional to spectral backscatter- 128
 ing $b_b(\lambda)$ and inversely proportional to absorption 129
 $a(\lambda)$ of the surface water column. 130

Water-leaving radiance, $L_w(\lambda)$ The component of the 131
 radiance signal measured above the water 132
 consisting of photons that have penetrated the 133
 water column and been backscattered out through 134
 the air-sea interface. It does not include photons 135
 reflected off the sea surface, also called sun glint. 136

Definition of the Subject, Relevance, Motivation 137

The oceans cover over 70% of the earth's surface and 138
 the life inhabiting the oceans play an important role in 139
 shaping the earth's climate. Phytoplankton, the micro- 140
 scopic organisms in the surface ocean, are responsible 141
 for half of the photosynthesis on the planet. These 142
 organisms at the base of the food web take up light 143
 and carbon dioxide and fix carbon into biological 144
 structures releasing oxygen. Estimating the amount of 145
 microscopic phytoplankton and their associated pri- 146
 mary productivity over the vast expanses of the ocean is 147
 extremely challenging from ships. However, as phyto- 148
 plankton take up light for photosynthesis, they change 149
 the color of the surface ocean from blue to green. Such 150
 shifts in ocean color can be measured from sensors 151
 placed high above the sea on satellites or aircraft and 152
 is called "ocean color remote sensing." In open ocean 153
 waters, the ocean color is predominantly driven by the 154
 phytoplankton concentration and ocean color remote 155
 sensing has been used to estimate the amount of chlo- 156
 rophyll *a*, the primary light-absorbing pigment in all 157
 phytoplankton. For the last few decades, satellite data 158
 have been used to estimate large-scale patterns of chlo- 159
 rophyll and to model primary productivity across the 160
 global ocean from daily to interannual timescales. Such 161
 global estimates of chlorophyll and primary productiv- 162
 ity have been integrated into climate models and illus- 163
 trate the important feedbacks between ocean life and 164
 global climate processes. In coastal and estuarine sys- 165
 tems, ocean color is significantly influenced by other 166
 light-absorbing and light-scattering components 167

168 besides phytoplankton. New approaches have been
169 developed to evaluate the ocean color in relationship
170 to colored dissolved organic matter, suspended sedi-
171 ments, and even to characterize the bathymetry and
172 composition of the seafloor in optically shallow waters.
173 Ocean color measurements are increasingly being used
174 for environmental monitoring of harmful algal blooms,
175 critical coastal habitats (e.g., seagrasses, kelps), eutro-
176 phication processes, oil spills, and a variety of hazards
177 facing the coastal zone.

178 Introduction

179 Remote sensing of ocean color allows for the determi-
180 nation of phytoplankton biomass and carbon fixation
181 over the global ocean. From these data, approximately
182 half of the global carbon fixation is estimated to occur
183 by ocean phytoplankton, accounting for roughly 50 Gt
184 C year⁻¹ [1, 2]. Phytoplankton are the base of the
185 marine food web, responsible for producing organic
186 carbon from carbon dioxide. The premise behind
187 ocean color remote sensing is to relate the intensity
188 and spectral distribution of visible light reflected out
189 of the water (“ocean color”) to the biological and
190 biogeochemical processes that influence the optical
191 properties of the water column (“bio-optical proper-
192 ties”) [3]. The distribution, abundance, and temporal
193 variation in various biological, physical, and chemical
194 processes can be observed synoptically from local and
195 regional to global spatial scales from sensors placed on
196 satellites or aircraft. Ocean color remote sensing pro-
197 vides long-term, continuous time series of phytoplank-
198 ton biomass and productivity data necessary for global
199 carbon cycle and climate research [4–6], but the uses of
200 ocean color data are increasingly diverse from military
201 to environmental monitoring applications [7].

202 Phytoplankton have a marked influence on the
203 subsurface and emergent light field [8]. The light
204 harvesting systems of phytoplankton, including the
205 chlorophyll *a* pigment which is ubiquitous among phy-
206 toplankton species, absorb light across the visible spec-
207 trum and influence the color of the near-surface ocean
208 [9]. An increase in absorption, or reduction in reflec-
209 tance, in the blue relative to the green portion of the
210 spectrum can be empirically related to chlorophyll *a*
211 concentration [10]. In other words, as phytoplankton
212 are added to the water column, more blue light is

213 absorbed and the reflected color changes from blue to
214 green. The advent of space-based ocean color sensors in
215 1978 with NASA’s Coastal Zone Color Scanner (CZCS)
216 and the follow on Sea-viewing Wide Field of View
217 Sensor (SeaWiFS) in 1997 greatly enhanced the under-
218 standing of phytoplankton distribution and concentra-
219 tion in the ocean [11]. Satellite ocean color imagery
220 provides estimates of phytoplankton abundance across
221 all ocean basins (Atlantic, Pacific, Indian, Arctic, and
222 Southern Oceans) and quantifies the variability from
223 seasonal to interannual timescales.

224 Over the last several decades, ocean color has
225 expanded beyond chlorophyll and a whole field has
226 emerged to study how the nature of the upwelling
227 light field changes as a function of the quantity and
228 composition of a variety of constituents in the near-
229 surface ocean, including biogenic and nonbiogenic
230 inorganic material, nonliving and living organic mate-
231 rial (i.e., phytoplankton, bacteria and viruses),
232 dissolved substances, and benthic habitats. Ocean
233 color research has sought to define the fundamental
234 relationship between the inherent optical properties of
235 the ocean, or the absorption and scattering properties
236 of the constituents, and water-leaving radiance. With
237 improved technology, including radiometers with bet-
238 ter spectral resolution, calibration, and a high signal-
239 to-noise ratio, and in situ optical instrumentation,
240 which provided a description of the optical properties
241 of oceanic constituents, biogeochemical parameters are
242 being estimated with greater accuracy and precision.
243 Ocean color remote sensing has moved beyond estima-
244 tions of chlorophyll alone and is now used to measure
245 total suspended sediment, colored dissolved organic
246 material, particulate inorganic carbon, and phyto-
247 plankton functional groups, as well as critical habitats
248 and hazards influencing pelagic and coastal waters.

249 Optical Properties of the Water Column

250 Scattering and absorption of photons, the basic unit of
251 light energy, in the surface ocean determines the inten-
252 sity and spectral shape of the water-leaving light signal
253 measured at an ocean color sensor. Photons that prop-
254 agate into the ocean interact with water molecules
255 dissolve and particulate matter and are either absorbed
256 or scattered. Because most of the light is propagated
257 downward into the water column, only a small amount

258 of the signal is scattered back out of the water column
259 and measured remotely. The bulk optical properties of
260 water are used to describe how the spectral and direc-
261 tional distribution of photons is altered within the
262 natural water body.

263 Inherent Optical Properties

264 The absorption and scattering properties of water mol-
265 ecules and the dissolved and particulate constituents
266 within the water are called inherent optical properties
267 (IOPs). IOPs do not depend on the ambient light
268 conditions, but are a function of the medium alone.
269 The two IOPs commonly used for remote sensing pur-
270 poses include the absorption (a) and scattering (b)
271 coefficients, which refer to the fraction of incident
272 light, a single, narrow, collimated beam of photons,
273 which is absorbed or scattered per unit distance within
274 the medium (units $1/\text{length}$ or m^{-1}). The scattering
275 coefficient stems from the volume scattering function
276 (β), which is the differential scattering cross section per
277 unit volume per solid angle, and is calculated as the
278 integral over all directions ($0-180^\circ$). The attenuation
279 coefficient (c) accounts for the reduction in light inten-
280 sity due to absorption and scattering processes
281 combined.

282 Both absorption and scattering processes can
283 change the color of the ocean as observed from
284 a satellite. Oceanic constituents that are primarily
285 responsible for absorption of photons include water
286 molecules, phytoplankton pigments, particulate detri-
287 tus, and *colored or chromophoric dissolved organic mate-*
288 *rial* (CDOM) (Fig. 1). Pure water is increasingly
289 effective at absorbing light at wavelengths greater than
290 550 nm and absorbs minimally in the blue and green
291 portion of the visible spectrum. Conversely, CDOM,
292 operationally defined as all of the colored material that
293 passes through a 0.2 μm filter, absorbs maximally in the
294 ultraviolet and blue portion of the spectrum, decreas-
295 ing exponentially with wavelength at a rate which is
296 related to the composition, or degradation state, of the
297 material. CDOM is generally comprised of humic and
298 fulvic acids and small colloidal material released
299 through the degradation of plant tissue, whether in
300 soils or in water [12, 13]. Commonly, CDOM is
301 modeled with an exponential function, but
302 a hyperbolic model may be more accurate [14].

Nonliving particulate material, called detritus or 303
tripton, absorbs in a manner similar to CDOM and 304
the two components are difficult to differentiate 305
spectrally. 306

Phytoplankton absorb light in a complex manner 307
related to the composition and quantity of their pho- 308
tosynthetic pigments, molecules structured to absorb 309
photons within the visible range of 400–700 nm, 310
dubbed photosynthetically available radiation or PAR. 311
There are three distinct classes of pigments, namely, 312
chlorophylls, carotenoids, and biliproteins. All phyto- 313
plankton contain chlorophyll a and most contain chlo- 314
rophylls b and/or c . Chlorophylls a , b , and c have two 315
strong absorption bands in the red and blue portions of 316
the spectrum. Chlorophyll a absorption is low in the 317
green (450–650 nm) portion of the spectrum. The 318
presence of chlorophylls b and c extend the range of 319
light available for photosynthesis further into both the 320
short- and long-wavelength regions. Carotenoid pig- 321
ments, of which there are many types (i.e., β -carotene), 322
extend absorption further yet into the short- 323
wavelength end of the green portion of the spectrum. 324
Finally, some phytoplankton contain red or blue pig- 325
ments called biliproteins, which are divided into classes 326
based on the position of their absorption peaks. The 327
phytoplankton absorption coefficient describes the 328
spectral absorption for natural waters comprised of 329
mixtures of phytoplankton and has been commonly 330
parameterized by chlorophyll concentration and dom- 331
inant cell size [15, 16]. 332

Scattering processes, which include *refraction*, 333
reflection and *diffraction*, occur at the boundary of 334
a particle with a different index of refraction, the ratio 335
of the speed of light in the surrounding medium to the 336
speed of light within the particle, than the surrounding 337
medium. Scattering is predominantly elastic, the energy 338
of the photon is conserved, but the direction of propa- 339
gation is altered. Rather than reducing light, scattering 340
works to inhibit the straight-path vertical penetration of 341
light. The total scattering coefficient (b) can be 342
subdivided into light which scatters in the forward 343
direction (b_f) ($0-90^\circ$) and the backward direction (b_b) 344
($90-180^\circ$) relative to the unattenuated beam. The 345
backscattered light is the radiance that is scattered out 346
of the water column and measured by a sensor as 347
“ocean color.” The magnitude of b_b is a function of 348

349 the concentration, composition (i.e., index of refrac-
 350 tion), shape, and size of particles [17].

351 Water molecules, salts, organic and inorganic par-
 352 ticles, and bubbles provide strong contributions to
 353 light scattering in the ocean. Scattering by pure water
 354 is the result of density fluctuations from the random
 355 motion of water molecules and has a wavelength
 356 dependence of λ^{-4} [18]. The presence of salt increases
 357 scattering, where pure seawater, with a salinity of
 358 35–38‰, scatters 30% more light than pure water
 359 devoid of salt. When particles are present, as in natural
 360 waters, scattering increases markedly [19]. The scatter-
 361 ing coefficient for the clearest surface waters is an order
 362 of magnitude greater than that of pure seawater. Partic-
 363 les that are large relative to the wavelength of light
 364 scatter mainly in the forward direction via diffraction,
 365 where photons propagating along the particle bound-
 366 ary change their direction in response to the boundary
 367 in a manner proportional to the cross-sectional area of
 368 the particle. Photons entering large particles are likely
 369 absorbed. Conversely, small particles mainly reflect and
 370 refract light in a manner proportional to the
 371 volume of the particle. Small particles with an index
 372 of refraction that deviates markedly from 1, including
 373 micron (10^{-6} m)-sized calcium carbonate plates or
 374 coccoliths generated by coccolithophorid phytoplank-
 375 ton ($n = 1.25$) or bubbles ($n = 0.75$), are highly efficient
 376 at scattering light in the backward direction [17].

377 The processes of absorption and scattering are con-
 378 sidered additive, therefore the sum of the contribution
 379 of each constituent determines the magnitude of the
 380 total coefficients a_t and b_t . As such, IOPs are separated
 381 into operationally defined components which com-
 382 prise a and b :

$$a_t = a_w + a_{ph} + a_d + a_g, \text{ and}$$

$$b_{bt} = b_{bw} + b_{bp}$$

383 where the subscripts correspond to water (w), algal or
 384 phytoplanktonic (ph), non-algal or detrital (d) matter,
 385 and dissolved material, originally termed “gelbstoff”
 386 (g). Dissolved material does not scatter light and the
 387 contributions of both algal and non-algal matter are
 388 generally consolidated into backscattering from partic-
 389 ulate (p) material. Recent advances in optical instru-
 390 mentation have allowed for the measurement of

absorption and scattering properties in situ and
 contributed to advances in ocean color remote
 sensing [20].

Apparent Optical Properties

Measurements of how light of different wavelengths
 attenuates with depth in the water column have been
 the historical basis of optical oceanography [21] fol-
 lowing from the use of white Secchi disks to water
 clarity. The properties that can be derived from mea-
 surements of ambient light in the water column are
 generally termed “apparent” optical properties (AOP)
 because they operate as optical properties describing
 the fundamental properties of the medium with only
 a slight dependence on the angular distribution of the
 light field. Spectral radiance, L , is the fundamental
 radiometric quantity which describes the spatial, tem-
 poral, directional, and wavelength-dependent structure
 of the light field in units of radiant flux per area per
 wavelength per solid angle ($\text{W m}^{-2} \text{nm}^{-1} \text{sr}^{-1}$) [18].
 Planar downwelling irradiance, E_d , is a measure of the
 radiant energy flux incident on the surface from all
 directions or solid angles contained in the upper hemi-
 sphere, with units of radiant flux per unit area per unit
 wavelength ($\text{W m}^{-2} \text{nm}^{-1}$). The same concept, applied
 to the lower hemisphere, describes upwelling irradi-
 ance, E_u . The ratio of the upwelling to downwelling
 irradiance yields *irradiance reflectance*, R , a measure of
 how much light of a certain wavelength entering the
 ocean is scattered backward by ocean molecules
 and particles.

For remote sensing purposes, only the radiance
 from a specific direction is measured by a sensor, not
 the entire upwelling irradiance. Hence, the color is
 parameterized as *remote sensing reflectance* (R_{rs} , sr^{-1}),
 which is the ratio of water-leaving radiance to
 downwelling irradiance. The term “water-leaving radi-
 ance” represents the radiance signal emerging from the
 water column in a nadir direction and specifically
 excludes those upward-directed photons that have
 only reflected off the sea surface and not penetrated
 the water column (i.e., sun glint). The term R_{rs} repre-
 sents the proportion of the downwelling light incident
 on the water surface that is returned through the air-
 water interface in the nadir direction due to differential

435 absorption and scattering processes. The parameter R_{rs}
436 is proportional to backscattering coefficient and
437 inversely proportional to absorption coefficient and
438 can be approximated as:

$$R_{rs} = \frac{f}{Q} \frac{b_b}{(a + b_b)}$$

439 where the ratio f/Q is related to the bidirectionality of
440 the light field and varies from 0.09 to 0.11 for most
441 remote sensing applications [22].

442 The rate of change of radiance and irradiance with
443 depth, known as the vertical diffuse attenuation coeffi-
444 cient (K ; m^{-1}), is another principle AOP. Irradiance
445 and radiance decrease approximately exponentially
446 with depth. The downward diffuse attenuation coeffi-
447 cient, K_d , the rate of decrease in downwelling irradi-
448 ance, $E_d(0)$, with depth (z),

$$E_d(z) = E_d(0)e^{-K_d z}$$

449 is commonly used in biological studies and is closely
450 linked to the absorption coefficient of the medium
451 specifically. The optical depth, ζ , corresponding to
452 any given physical depth is defined below:

$$\zeta = K_d z$$

453 Optical depths frequently used by biologists include
454 2.3 and 4.6, corresponding to the 10% and 1% light
455 levels, respectively. Also, the portion of the surface
456 water column contributing 90% of the water-leaving
457 radiance has a depth, z , described by $z = 1/K_d$ [12].
458 The radiative transfer equation is the mathematical
459 formulation that defines the relationship between the
460 optical properties of natural water bodies [18] and is
461 the basis for the semi-analytical models used in ocean
462 remote sensing.

463 Basics of Ocean Color Remote Sensing

464 Many challenges are inherent to remote sensing of
465 ocean color. In comparison to land, the ocean target
466 is dark, with an albedo of only a few percent. This
467 means that most of the light that enters the water is
468 propagated downward into the water column and only
469 a few percent is scattered back out again. This is quite
470 different from land and ice surfaces which have a much
471 higher albedo. Most ocean color sensors are passive in
472 that they measure only the radiation that originates

473 from the sun, as opposed to active sensors that produce
474 and sense their own stream of light (e.g., Light Detec-
475 tion and Ranging or LIDAR). Viewed from space,
476 moreover, the ocean is observed through a thick atmo-
477 sphere which reflects sunlight back to the sensor and is
478 significantly brighter in the visible wavelengths than
479 the water itself. In technical terms, this is quantified
480 as a low signal-to-noise ratio where the “signal” is the
481 light reflected from within the ocean and the “noise” is
482 light reflected from the atmosphere and sea surface.
483 This section outlines the platforms, calibration, atmo-
484 spheric correction, and levels of data processing critical
485 for successful ocean color remote sensing.

486 Sensors and Platforms

487 Ocean color sensors can be mounted on space-based
488 satellites or on suborbital platforms like aircraft or
489 unmanned aerial vehicles. The spatial and temporal
490 sampling and the questions that can be addressed
491 with the data depend on the type of platform
492 employed. Most current ocean color sensors have
493 a wide field of view, which translates to a wide sampling
494 swath, and are mounted on sun synchronous polar-
495 orbiting satellites (e.g., CZCS, SeaWiFS, MODIS Aqua
496 and Terra). These sensors have the potential to provide
497 global coverage of the earth roughly every 3 days at the
498 equator and more frequently at the poles. However,
499 clouds obscure the ability of the sensor to view the
500 ocean color and, in reality, temporal sampling for any
501 given region is much less. Data are frequently averaged
502 over longer time periods to produce weekly, monthly,
503 and seasonal composite images of the global ocean
504 (Fig. 2). The spatial resolution is also limited nominally
505 to 1 km pixel widths (and down to 500 m for select
506 channels) in these polar-orbiting sensors in part
507 because of limitations in the signal-to-noise ration
508 inherent to the dark ocean surfaces (see atmosphere
509 correction below). Global datasets are often aggregated
510 to 4-km or 9-km pixels. However, higher spatial reso-
511 lution on the scale of meters can be obtained from
512 some space-based platforms and from ocean color sen-
513 sors placed on aircraft (Fig. 3).

514 The current suite of ocean color sensors has nomi-
515 nally six to seven spectral bands spanning the visible
516 wavelengths (400–700 nm). These bands are not spread
517 uniformly across the visible spectrum, but have been

518 selected to correspond to reflectance characteristics of
519 open ocean waters, particularly those related to phyto-
520 plankton pigment absorption features. Three bands are
521 generally found in “blue” (near 410, 440, and 490 nm),
522 one to two bands in “green” (510 or 530, 560 nm), and
523 one to two channels in the “red” (670, 680 nm). In
524 addition, channels are also incorporated in the near
525 infrared (NIR) to short-wave infrared (SWIR) for
526 purposes of atmospheric correction (see section
527 “Atmospheric Correction”). Most of the visible chan-
528 nels were selected to match absorption features of phy-
529 toplankton and other constituents. Additional
530 channels are also needed to bridge the large 100 nm
531 gap between 560 and 670 nm, where absorption fea-
532 tures are dominated by water, to better constrain back-
533 scattering in complex coastal waters [23, 24]. New
534 technology has allowed for the development of sensors
535 that span the full range of visible and near infrared
536 (NIR) spectrum or “hyperspectral,” also referred to as
537 imaging spectrometers.

538 No single platform is ideal for addressing all of the
539 temporal and spatial variability in the oceans.
540 A constellation of ocean color imagers with comple-
541 mentary capabilities and specifications is ultimately
542 required to adequately address the diverse require-
543 ments of the coastal research and applied user commu-
544 nities. For example, the Hyperspectral Imager for the
545 Coastal Ocean (HICO) was recently installed on the
546 International Space Station for the study of the coastal
547 ocean and adjacent lands. This imaging spectrometer is
548 intended to provide hyperspectral imagery at 100-m
549 resolution sampling at different angles and times of the
550 day for selected regions. Sensors are also being consid-
551 ered for placement on geostationary satellites, similar
552 to the international constellation of meteorological
553 satellites. Such sensors would look at the same regional
554 location on earth for extended periods of time and be
555 able to provide better temporal resolution of ocean
556 processes and episodic hazards. Regional efforts such
557 as the Geostationary Ocean Color Imager (GOCI) on
558 the COMS-1 platform from South Korea are already
559 planned for launch. In addition, higher spatial and
560 spectral resolution polar orbiting sensors are proposed
561 to address questions related to seasonal variability in
562 global coastal habitats and polar ice cover.

563 Portable sensors flown on aircraft or unmanned
564 aerial vehicles (UAV’s) provide a critical sampling

565 niche distinct from satellite-borne sensors that is partic-
566 ularly well suited for coastal applications and ice
567 research (Fig. 3a) [25]. Airborne sensors can sample
568 at finer spatial scales (meters), can operate under
569 clouds and with nearly unlimited repeat coverage, and
570 are effective platforms for high-resolution active sen-
571 sors (e.g., LIDAR). Flight lines and scanning geome-
572 tries can also be oriented to avoid sun glint and their
573 range can be greatly expanded by launching from ships.
574 The technology required to build portable sensors for
575 coastal applications is developing with wide field of
576 views, minimum polarization dependence, high
577 response uniformity, and optimized signal-to-noise
578 ratio for low-light channels [26, 27]. These sensors
579 are becoming more popular for use in the environmen-
580 tal management of coral reefs, seagrasses, kelps, and
581 other coastal targets, and have the potential to monitor
582 episodic events such as harmful algal blooms and run-
583 off and flooding from storms.

584 Ocean color sensors in space have traditionally been
585 “whisk broom” in design where a single detector col-
586 lects data one pixel at a time as the telescope rotates to
587 build up pixels along a scan line. Some satellites and
588 most of the suborbital sensors are “pushbroom” where
589 the entire scan line is imaged synoptically by a line of
590 sensors arranged perpendicularly to the flight direc-
591 tion. In order to achieve high-quality data that can
592 track climatological trends in ocean color, sensors are
593 required to have very high radiometric accuracy and
594 stability. Detectors are calibrated pre- and post-launch
595 and degradation over time is carefully quantified with
596 vicarious calibrations from field measurements and
597 ideally lunar imaging. Periodic reprocessing of the
598 satellite data is considered critical to obtaining
599 high-quality datasets and continuity over multiple
600 missions [5, 28].

601 Atmospheric Correction

602 One of the most challenging aspects of ocean color
603 remote sensing is successfully removing the atmo-
604 spheric signal from the water column signal. Aerosols
605 and gas molecules are the primary contributors to the
606 radiance measured at the top of the atmosphere.
607 Approximately 80–85% of the radiance measured at
608 the sensor is the result of Rayleigh scattering by mole-
609 cules in the atmosphere that are small relative to the

610 wavelength of light. Photons reaching the sensor (L_u)
611 are a combination of those scattered by the atmosphere
612 (L_p), reflected at the air-water interface (L_r), known as
613 specular reflection, or have been backscattered from
614 within the water column, dubbed water leaving radi-
615 ance, or L_w (Fig. 4). The water-leaving radiance, used
616 for most ocean color applications, is only a small por-
617 tion of the signal retrieved at a satellite and must be
618 differentiated from the photons scattered within the
619 atmosphere and specularly from the sea surface in
620 a process called “atmospheric correction.”

621 Rayleigh scattering, which decreases with wave-
622 length (λ) following λ^{-4} , can be estimated using
623 a single-scattering radiative transfer equation using
624 the atmospheric pressure and appropriate viewing
625 geometry [29]. An additional 0–10% of the radiance
626 signal is due to aerosols (i.e., haze, dust, and pollution),
627 particles with sizes comparable to the wavelength
628 of light which absorb and scatter as a complex function
629 of their type, size, and concentration. The type and
630 concentrations of aerosols overlying the ocean are
631 quite variable in space and time, particularly in coastal
632 regions subject to urban pollution and terrestrial
633 dust [30].

634 Atmospheric correction of aerosols remains
635 a challenge for accurately deriving water-leaving radi-
636 ance from satellites and aircraft. Approaches generally
637 focus on channels in the NIR and even in the short
638 wave infrared (SWIR) [29, 31, 32]. Because water
639 absorbs so heavily in the infrared, very few photons
640 are reflected out of water in this part of the electromag-
641 netic spectrum and the signal is dominated by reflec-
642 tion from atmospheric gases and aerosols. Various
643 types of models are used, including coupled models
644 and multi-scattering models, to infer the contribution
645 of aerosol reflectance in the visible portion of the
646 spectrum from the infrared. Aerosol reflectance is not
647 spectrally flat, but varies with wavelength, and at least
648 two channels are necessary to determine the spectral
649 shape of aerosol reflectance and extrapolate from the
650 NIR to visible wavelengths [29, 33].

651 Dust, particularly from desert storms, can also
652 impact the optical properties of the atmosphere and
653 most atmospheric correction algorithms for ocean
654 color sensors are not capable of handling absorbing
655 mineral dust (i.e., colored dust) [34]. For example,
656 airborne plumes of Saharan dust are observable all

657 year on satellite images over the Tropical Atlantic and
658 may be increasing in areas like the Mediterranean Sea
659 [35]. If colored dusts are not properly corrected for in
660 the atmospheric correction schemes, then the color of
661 the ocean is not properly estimated resulting in errors
662 in chlorophyll and other biogeochemical properties
663 retrieved from the satellite data [36]. In addition to
664 its radiative impact, it has been suggested that this
665 mineral dust has a substantial influence on the marine
666 productivity and may also carry pollutants to the
667 oceans [37, 38].

668 Whitecaps breaking on the sea surface must also be
669 corrected from derivations of water-leaving radiance.
670 Whitecap reflectance is often modeled using an empir-
671 ical cubic relationship to wind speed and an approxi-
672 mate reflectance value for an individual whitecap [39],
673 but such models often overcorrected the imagery, and
674 a fixed whitecap correction is often applied when wind
675 speeds exceed a threshold (e.g., 8 m s^{-1} for SeaWiFS).
676 At high winds, some of the signal attributable to white-
677 caps is removed by the aerosol corrections.

678 Levels of Processing

679 Standards for ocean color data processing, developed at
680 US National Aeronautics and Space Administration
681 (NASA) for the SeaWiFS mission [40], are widely
682 followed by the international community of
683 ocean color users and involve four levels of processing
684 (Table 1). Au2

685 Ocean Color Algorithms

686 This section presents the classification of the global
687 ocean into two optical classes: Case 1 and Case 2 and
688 then proceeds to present the general approaches or
689 algorithm for two of the main products from ocean
690 color imagery, chlorophyll and primary productivity,
691 for Case 1 waters and to describe the semi-analytical
692 algorithms which can be used for both Case 1 and
693 Case 2 waters.

694 Optical Classification of Aquatic Systems

695 Ocean waters have long been classified based on their
696 color properties [41]. A classification system intro-
697 duced in 1977 differentiates phytoplankton-dominated
698 waters from those where inorganic particles are

699 dominant, known as Case 1 and Case 2, respectively
700 [42]. These cases have evolved from their original
701 forms into the categories used today: Case 1 waters
702 are those waters where optical properties are deter-
703 mined primarily by phytoplankton and related colored
704 dissolved organic matter (CDOM) and detritus degra-
705 dation products; Case 2 waters are waters where optical
706 properties are significantly influenced by other constitu-
707 ents such as mineral particles, CDOM, or
708 microbubbles that do not covary with the phytoplank-
709 ton concentration [8, 43]. In today's world, approxi-
710 mately 97% of the surface ocean falls toward the
711 optically simple, deep water, Case 1 classification.
712 When inorganic, organic, particulate, and dissolved
713 material all vary independently of one another, such
714 as in coastal ecosystems with considerable riverine
715 influence, bottom resuspension, or optically shallow
716 regions, the system falls toward the Case 2 classifica-
717 tion, also called "optically complex."

718 This binary classification scheme has been prevalent
719 in bio-optical modeling of ocean waters and develop-
720 ment of ocean color algorithms. However, many
721 problems exist with use of such simplified schemes in
722 modeling natural systems. For example, there is no
723 sharp dividing line between the cases and each investi-
724 gation tends to use as different criteria for defining
725 Case 1 and Case 2. Commonly the two cases are defined
726 by the relationship between chlorophyll and remote
727 sensing reflectance or scattering. Even in the global
728 ocean considered to be Case 1, CDOM concentrations
729 do not covary with the instantaneous chlorophyll con-
730 centration [44], but can vary from 30% to 60% of the
731 total non-water light absorption [45] and result from
732 differences in water mass ventilation, water column
733 oxidative remineralization, and photobleaching [46].

734 In *optically shallow waters*, in addition to the water
735 column and its constituents (i.e., dissolved and partic-
736 ulate material), the bottom contributes to the water
737 leaving radiance in a way that depends on the bottom
738 composition and roughness. Periodic measurements of
739 bottom types using passive remote sensing in coastal
740 systems are valuable for describing and monitoring
741 habitats [47]. The magnitude and spectral quality of
742 light reflected off of the bottom material can allow
743 separation of bottom reflectance from the water col-
744 umn signal, where different bottom types will have
745 a different effect on reflectance. Shallow, clear water

will yield the most information about bottom material, 746
more readily allowing spectral discrimination of 747
bottom type. However, as depth and the diffuse atten- 748
uation coefficient, K_{db} , increase, the bottom signal 749
becomes difficult to differentiate. 750

Empirical Chlorophyll Algorithms 751

Standard calculation of chlorophyll from ocean color 752
imagery involves an empirical relationship developed 753
from field observations collected throughout the global 754
ocean [10]. Algorithms are typically not developed 755
from the remotely sensing imagery itself, because this 756
would incorporate any biases in calibration and atmo- 757
spheric correction procedures used to derive reflect- 758
tance, as well as any spatial inhomogeneity in 759
parameters over pixel scales, and would require new 760
algorithms for every new calibration and reprocessing, 761
as well as launch of new sensor. Empirical solutions are 762
used because an analytical solution to the problem 763
requires an assessment of the entire radiance distribu- 764
tion and depth derivative and such measurements are 765
not possible with remote sensing [48]. Only the 766
upward flux incident upon the water-air interface at 767
angles less than 48° , the angle at which complete inter- 768
nal reflection occurs, is measurable from above the sea 769
surface [6] and generally only the flux emitted in 770
a single viewing angle is remotely sensed. 771

The current empirical algorithms use the shift in 772
ocean color from "blue" at low Chl, where R_{rs} peaks at 773
400 nm, to "green" at high chlorophyll, where R_{rs} peaks 774
at 555 nm (Fig. 5a). Empirical ocean color algorithms 775
have been applied to the vast majority of the global 776
ocean considered Case 1 and use multiple ocean color 777
bands typically log-transformed and in a ratio formu- 778
lation to minimize problems with atmospheric correc- 779
tion and differential scattering in the ocean. The 780
coefficients for the algorithms are regularly adjusted 781
to account for different sets of wavebands in various 782
sensors and as new field data becomes available 783
(Table 2). The OC3M algorithm developed for 784
MODIS, for example, uses a 4th order polynomial 785
derived from a large global dataset of field measure- 786
ments of chlorophyll and R_{rs} . It uses a logarithmic ratio 787
of blue light (either 443 and 488 nm depending on 788
which is greater) to green light (555 nm) and follows 789
an inverse relationship such that low Chl is retrieved or 790

791 high ratios when the ocean color is blue and high Chl
792 when more green light is reflected (Fig. 5b). These types
793 of algorithms tend to work best at lower Chl
794 ($<1 \text{ mg m}^{-3}$), found in most of the world ocean,
795 where the algorithm has a flatter slope [49].

796 For much of the open ocean where chlorophyll
797 concentrations are low, the empirical algorithms work
798 well and relative error is estimated to under 35% [50].
799 However, empirical derivations of chlorophyll in Case 1
800 waters can be in error by a factor of 5 or more, partic-
801 ularly at higher Chl [49]. Such variability is due to
802 differences in absorption and backscattering properties
803 of phytoplankton and related concentrations of colored
804 dissolved organic matter (CDOM) and minerals. The
805 empirical algorithms have built-in assumptions that
806 follow the basic precept of biological oceanography;
807 i.e., oligotrophic regions with low phytoplankton bio-
808 mass are populated with small phytoplankton while
809 more productive regions contain larger bloom-
810 forming phytoplankton. With a changing world
811 ocean, phytoplankton composition may shift in
812 response to altered environmental forcing and
813 CDOM and mineral concentrations may become
814 uncoupled from phytoplankton stocks creating further
815 uncertainty and error in the empirical approaches [49].

816 The empirical approach is not widely applicable in
817 Case 2 waters, generally found near the coasts. Such
818 waters are influenced by freshwater plumes with
819 CDOM and minerals that significantly impact the opti-
820 cal properties, as well as resuspension of bottom sedi-
821 ments [51]. Phytoplankton assemblages can also be
822 diverse in coastal regimes and light absorption per
823 unit of Chl is difficult to constrain. Melting and runoff
824 of glacial sources can increase particle concentrations
825 in the nearshore and change phytoplankton assem-
826 blages. In order to use remote sensing in coastal waters,
827 semi-analytical models are employed that are able to
828 decompose the reflected color into the many absorbing
829 and scattering constituents in the water column
830 (see Section “Semi-analytical Algorithms”).

831 Primary Productivity Algorithms

832 Net primary production is a key parameter derived
833 from ocean color data that provides a measure of how
834 much carbon dioxide is taken up and incorporated into
835 ocean phytoplankton during photosynthesis. Export of

fixed carbon to the ocean interior, while only a fraction 836
of the total biomass produced, provides a long-term 837
sink for atmospheric carbon dioxide [52]. While satel- 838
lite-derived Chl is not a direct measure of carbon fixa- 839
tion in phytoplankton, such estimates are typically 840
derived from correlates of Chl and rates of carbon 841
fixation [53]. Net primary productivity varies with 842
phytoplankton species assemblages and their physio- 843
logical state related to light, temperature, nutrients, 844
and other environmental factors. 845

A variety of formulations have been developed for 846
ocean color remote sensing and parameterized for the 847
global ocean or specific regions. Models are generally 848
restricted to parameters that can also be globally 849
derived from remote sensing imagery, such as sea sur- 850
face temperature and photosynthetically available radi- 851
ation (PAR). Moving from a standing stock of 852
phytoplankton biomass to photosynthetic rate requires 853
a time-dependent variable. Solar radiation in the form 854
of PAR is commonly used in formulations to convert 855
biomass to primary productivity. The physiological 856
response of the measured chlorophyll to light, nutri- 857
ents, temperature, and other environmental variables 858
must also be incorporated in the model. Primary pro- 859
ductivity models can be differentiated by the degree of 860
explicit resolution in depth and irradiance [53]. 861

Round robin experiments have been conducted to 862
compare the performance of models for assessing 863
global productivity from ocean color imagery, as well 864
as the output from ecosystem-based general circulation 865
models [1, 54]. The third such effort found that global 866
average primary productivity varied by a factor of two 867
between models and the global mean productivity for 868
the different model groups ranged from 44 to 57 Gt 869
C year⁻¹ with an average of 50.7 Gt C year⁻¹. The 870
models diverged the most in the high-nutrient low 871
chlorophyll waters of the Southern Ocean. Primary 872
productivity algorithms have also been formulated 873
from remote sensing estimates of the inherent optical 874
properties (such as light absorption and backscatter- 875
ing) directly [55, 56], without incorporating Chl and 876
the associated uncertainties inherent in that parameter. 877

878 Semi-analytical Algorithms

The empirical algorithms used for deriving chlorophyll 879
have been likened to a “black box” that provides no 880

881 mechanistic understanding of ocean optics and are
882 particularly challenging to apply in a changing ocean,
883 when the water properties are different from the
884 empirical data used to develop the formulation [57].
885 Analytical solutions to deriving IOPs from water-
886 leaving radiance are not possible because the radiance
887 can only be measured from a few angles. Semi-
888 analytical algorithms (or “quasi-analytical”) are based
889 on a fundamental understanding of the propagation of
890 light in the ocean and provide a more mechanistic
891 approach to ocean color. These algorithms incorporate
892 some empirical approximations, but do not rely on
893 fixed predetermined relationships between the absorp-
894 tion and backscattering components of the water
895 column.

896 In semi-analytic models, the ocean color signal is
897 inverted to obtain estimates of the various absorbing
898 and backscattering constituents directly. Parameteriza-
899 tion of how water, phytoplankton, and dissolved and
900 detrital material inherently absorb and backscatter
901 light across the visible spectrum (i.e., their spectral
902 shape) is used in these models. The spectral reflectance
903 measured at the satellite is often inverted to retrieve the
904 amounts of each individual component contributing to
905 the absorption and backscattering of light. Such algo-
906 rithms are the primary methods for obtaining CDOM
907 distributions across the ocean surface [58]. In semi-
908 analytical models, the biogeochemical parameters,
909 such as Chl and total suspended matter, are derived
910 secondarily from the IOPs. Semi-analytical formula-
911 tions vary in terms of their architecture and statistical
912 methods employed to retrieve the inherent optical
913 properties from the remote sensing signal, and the
914 empirical parameterizations within the models [57].

915 **Applications for Oceanography**

916 Ocean color remote sensing is an important tool for
917 many branches of oceanography, including biological,
918 physical, and chemical oceanography. The section
919 below summarizes only some of the main applications
920 of ocean color remote sensing with the understanding
921 that the uses of ocean color are continuously
922 expanding. A recent monograph from the Interna-
923 tional Ocean Color Coordinating Group (IOCCG)
924 entitled “Why Ocean Colour?: The Societal Benefits of
925 Ocean-Colour Technology” extensively documents the

926 many uses of ocean color remote sensing from scien-
927 tists to environmental managers to the general public
928 [7]. Web-based software has also been developed, see,
929 e.g., Giovanni [59], which allows the public to freely
930 map and analyze ocean color imagery over time and
931 space. Figure 6 provides an example of various types of
932 figures that can be easily generated from remotely
933 sensed chlorophyll using that software.

Biological Oceanography

934
935 Apart from estimating chlorophyll and primary pro-
936 ductivity, ocean color remote sensing has many biolog-
937 ical applications that range from phytoplankton
938 physiology to assessing distributions of migrating
939 whales. Phytoplankton physiology, particularly the effi-
940 ciency of light capture and utilization, has been
941 modeled from the natural fluorescence signature pro-
942 vided by ocean color remote sensing [60]. Even though
943 the spectral resolution available in most current ocean
944 color satellite is limited to six to eight available spectral
945 channels [61], a variety of phytoplankton taxa and
946 groups have also been distinguished from satellite
947 imagery based on their unique optical properties and/
948 or regional tuning of algorithms using knowledge of
949 the local phytoplankton composition. Phytoplankton
950 taxa can have unique sets of accessory pigments that
951 differentiate them from one another and can result in
952 unique absorbance spectra. In addition, phytoplankton
953 can have cell walls or exterior plates comprised of
954 different materials (e.g., silica, calcium carbonate)
955 that can make them more or less reflective. Various
956 approaches have been developed to map size classes
957 (from pico- to microplankton) or major groups of
958 phytoplankton in the global ocean [62]. Other algo-
959 rithms have targeted particular phytoplankton taxa
960 such as coccolithophores, nitrogen-fixing
961 *Trichodesmium* [63], toxic dinoflagellates [64], and
962 nuisance cyanobacteria [65].

963 Satellite-derived chlorophyll and primary produc-
964 tivity provide a key metric to assess marine ecosystems
965 temporally on a global scale and have been used exten-
966 sively to monitor conditions that impact other biolog-
967 ical organisms in the sea. The relationship between
968 satellite-derived chlorophyll data and organisms at
969 higher trophic levels depends upon the number of
970 linkages in the food web. For species like anchovies

971 and sardines, which eat phytoplankton in their life
972 cycle, the linkage can be direct [66]; whereas, many
973 trophic levels can exist for other species and the rela-
974 tionship can be quite nonlinear [7]. The distribution,
975 movement, and migration of whales, dolphins, pinni-
976 peds, penguins, and sea turtles has been related, either
977 directly or indirectly, to remotely sensed patterns of Chl
978 (reviewed in [7]). Most fish have planktonic larval
979 stages that are strongly influenced by ocean circulation
980 and recruitment success has been found to be related to
981 the degree of timing between spawning and the sea-
982 sonal phytoplankton bloom, as observed from satellites
983 [67]. Ocean color remote sensing has also been used to
984 study invertebrates in the global ocean, such as shrimp
985 in the Newfoundland-Labrador Shelf [68] and ptero-
986 pods and pelagic mollusks in the Ross Sea [69]. Mean
987 net primary productivity, determined from ocean color
988 satellite imagery, elucidates species richness in biogeo-
989 graphical studies of cephalopods [70].

990 New techniques have also been developed to use
991 ocean color remote sensing in optically shallow water
992 systems to deduce changes in benthic habitats [71].
993 Optically shallow water occurs when the seafloor con-
994 tributes to the reflectance signal observed remotely by
995 a satellite (Fig. 7a) and is defined by a combination of
996 water clarity, water depth, and bottom composition.
997 Satellite estimates of biomass and net productivity of
998 seagrasses, kelps, and other benthic producers have
999 been conducted over regional scales [47, 72] (Fig. 7b).
1000 Ocean color imagery from aircraft can map fine-scale
1001 distributions of seagrasses, coral reefs, and other coastal
1002 habitats at local scales [73, 74]. Changes in ocean color
1003 signals over time can also be used to assess contribu-
1004 tions of coastal carbon to the global carbon cycle [75,
1005 76]. Responses of coastal regions linked to terrestrial
1006 changes can also be observed with ocean color imagery.
1007 Warming of the Eurasian landmass, for example, has
1008 led to enhanced productivity in the water column [77].
1009 Agricultural runoff from fields in Mexico was shown to
1010 stimulate large phytoplankton blooms in the Gulf of
1011 California that alter water clarity and potentially lead to
1012 anoxic conditions [78].

1013 Ocean Physics

1014 Ocean color data is well suited to the detection of
1015 convergence zones and oceanic fronts, sometimes

1016 better than thermal sensors which penetrate only the
1017 skin layer, or the first 10 μm , of the water column.
1018 Interestingly, a sequence of ocean-color-derived chlo-
1019 rophyll images may help predict the formation of
1020 eddies days before they appear. The increased penetra-
1021 tion of visible radiation reveals more frontal features
1022 and with greater detail than those retrieved with sea
1023 surface temperature data alone [79]. Likewise, upwell-
1024 ing regions, which bring cold, nutrient-rich waters up
1025 to the surface can be readily identified in ocean color
1026 images as areas with an enhanced chlorophyll concen-
1027 tration. The intensity of upwelling from year-to-year
1028 can be tracked through the time series of chlorophyll
1029 abundance. Chlorophyll is an effective indicator for
1030 detecting anomalous activity in the oceanic environ-
1031 ment. Evidence of an El Niño event beginning in
1032 November of 1997, during which phytoplankton pig-
1033 ment concentrations appeared anomalously low in the
1034 Equatorial Upwelling Zone, was obvious in the contin-
1035 uous coverage supplied by SeaWiFS. The onset of
1036 restored upwelling was likewise evident with the
1037 increased chlorophyll concentrations during the
1038 months of June and July 1998 [80].

1039 Ocean water clarity also affects the distribution of
1040 shortwave heating in the water column. Both chloro-
1041 phyll and CDOM concentrations have been linked to
1042 changes in heating of surface waters [81, 82]. Increased
1043 clarity would be expected to cool the surface and heat
1044 subsurface depths as shortwave radiation penetrates
1045 deeper into the water column. Recent studies show
1046 that water clarity, as determined from ocean color
1047 remote sensing, is an important feature in atmospheric
1048 circulation (the Hadley cells), oceanic circulation
1049 (Walker Circulation), and formation of mode water
1050 [83]. Importantly, ocean color imagery is also critical
1051 to predicting tropical cyclone activity. The presence of
1052 light-absorbing constituents (like Chl and CDOM)
1053 shapes the path of Pacific tropical cyclones and propa-
1054 gation to higher latitudes [84].

1055 Chemical Oceanography

1056 A major contributor to the ocean carbon system is
1057 colored dissolved organic material (CDOM),
1058 a mixture of compounds produced primarily by
1059 decomposition of plant matter. CDOM, when present
1060 in high enough concentrations, produces a yellow or

1061 brownish color and is highly reactive in the presence of
1062 sunlight. When CDOM undergoes photodegradation,
1063 organic compounds essential to phytoplankton and
1064 bacterial growth are released [85]. Satellite measure-
1065 ments collected using SeaWiFS, MODIS, and MERIS
1066 produce daily estimates of CDOM at 1 km resolution.
1067 High temporal resolution CDOM maps can be used to
1068 identify and track water masses at timescales close to
1069 the processes determining its distribution. CDOM
1070 dynamics plays an important role in ocean biogeo-
1071 chemistry, regulating the absorption of blue and UV
1072 radiation in the surface ocean and therefore altering the
1073 depth of the euphotic zone [58] and heating surface
1074 waters [82]. Although CDOM is difficult to analyze
1075 chemically, its distribution and abundance, identifiable
1076 using ocean color remote sensing, is highly relevant to
1077 understanding carbon cycling in the ocean.

1078 The particulate inorganic carbon (PIC) pool, cal-
1079 cium carbonate (CaCO_3), contributes substantially to
1080 the ocean carbon cycle and ocean color reflectance.
1081 Calcification reduces surface carbonate, decreasing
1082 alkalinity. Organic carbon production via photosyn-
1083 thesis counterbalances this effect. Coccolithophores,
1084 haptophyte algae, are responsible for the majority of
1085 the biogenic particulate inorganic carbon production.
1086 Coccolithophores generate and shed tiny white plates
1087 of calcium carbonate called coccoliths, which are highly
1088 efficient at reflecting light, ultimately producing large
1089 turquoise patches in the ocean readily visible in ocean
1090 color imagery [86]. Ocean color remote sensing algo-
1091 rithms have been formulated for generating quantita-
1092 tive estimates of particulate inorganic carbon and
1093 calcification rates on regional and global scales [87,
1094 88]. A continued, long-term assessment of
1095 coccolithophore and particulate inorganic carbon
1096 abundance from satellite imagery will aid in under-
1097 standing the impact of ocean acidification on marine
1098 organisms reliant on carbonate for the formation of
1099 shells [89].

1100 Ocean color imagery provides the ability to expand
1101 small-scale biogeochemical studies to regional or global
1102 scales. For example, the marine inorganic carbon cycle
1103 has been shown to be not only influenced by marine
1104 plankton but also by fish that precipitate carbonates into
1105 the surface waters. Extrapolations from satellite-derived
1106 net primary productivity up several trophic levels to

1107 marine fish [90] reveal that fish may contribute
1108 3–15% of the total oceanic carbon production [91].

1109 **Applications for Environmental Monitoring**

1110 Ocean color remote sensing plays a major role in mon-
1111 itoring and sustaining the health and resilience of
1112 marine ecosystems, including fisheries and endangered
1113 species [40]. Ocean color products are helping to
1114 address how environmental variability influences affect
1115 annual recruitment of fish stock [92] and to locate and
1116 manage fisheries [7]. Ocean color imagery coupled
1117 with other remote sensing products such as sea surface
1118 temperature is a fundamental tool in ecosystem-based
1119 management of marine resources [93].

1120 Ocean color remote sensing can monitor a variety
1121 of acute and chronic hazards influencing the oceans
1122 including: harmful algal blooms, oil spills, coastal
1123 flooding, icebergs and marine debris [7].
1124 A combination of ocean color, field, and meteorologi-
1125 cal datasets have been critical in identifying the onset of
1126 harmful algal blooms (HABs), which can produce
1127 toxins and create hypoxic conditions. While toxins
1128 cannot be directly observed from ocean color, the
1129 onset of potential harmful blooms can be identified
1130 using a chlorophyll anomaly method [94] in concert
1131 with other forecasting tools such as field and meteor-
1132 ological datasets. This information can then be passed
1133 on to coastal managers and state agencies to put strat-
1134 egies in place to deal with an impending bloom. A long-
1135 term time series of ocean color products can aid in
1136 elucidating forcing and transport mechanisms of
1137 these harmful blooms and help improve predictability.

1138 New techniques are being developed for early detec-
1139 tion, containment, and clean up of oil spills. Remote
1140 sensing can be used to detect oil spills that can change
1141 surface reflectance properties and the color of the ocean
1142 [95]. Coarse spatial and temporal resolution, limited
1143 spectral bands, cloud-cover issues and high sunlight
1144 requirements have generally restricted the usefulness
1145 of ocean color imagery for oil-spill detection
1146 from polar orbiting satellites [96]. Moreover,
1147 current processing methods may not allow data
1148 availability within hours of data capture. The spatial,
1149 temporal, and spectral resolution needed for oil
1150 spill recovery planning requires high-resolution,

1151 hyperspectral ocean color radiometers deployed in
1152 geostationary orbit [40].

1153 Ocean color imagery has also been used to track
1154 marine debris on the ocean surface which can entangle
1155 a variety of pelagic species, such as endangered sea
1156 turtles, seals, and whales. The nets also become
1157 ensnared on coral reefs and damage the reef structure
1158 and associated organisms that require a healthy reef
1159 ecosystem [97, 98]. Satellite ocean color data are part
1160 of the methods being developed to locate and identify
1161 potential locations of marine debris to aid their
1162 removal from these ecosystems.

1163 Ocean color imagery is also useful in monitoring
1164 water quality in inland aquatic water bodies. Nuisance
1165 algal blooms, such as cyanobacteria, cause aesthetic
1166 degradation to lakes and reservoirs resulting in surface
1167 scum, unpleasant taste and odor in drinking water
1168 (from the production of metabolites such as methyl
1169 isoborneol and geosmin), and possible adverse effects
1170 to human health from blue-green algal toxins.
1171 Predicting the locations and timing of blue-green
1172 algal bloom using traditional sampling techniques is
1173 difficult and hyperspectral remote sensing can be an
1174 important tool in such monitoring efforts [99].

1175 **Future Directions**

1176 Within a few decades, the ability to view the global
1177 ocean color regularly through remote sensing has rev-
1178 olutionized the perceptions about ocean processes and
1179 feedbacks to the earth's climate. The decade of contin-
1180 uous ocean color imagery has provided a foundation
1181 for assessing change in the earth's systems and long-
1182 term averages or "climatologies" of products, such as
1183 chlorophyll, CDOM, and PIC, have been produced to
1184 provide a baseline of ocean biogeochemistry (Fig. 8).
1185 The products obtained from ocean color are now incor-
1186 porated into all domains of oceanography, global cli-
1187 mate forecasts, military applications, and
1188 environmental monitoring across the expansive global
1189 ocean and the vulnerable coastal regions where most of
1190 the human population resides [11]. While successful,
1191 the technology and processing of ocean color remote
1192 sensing is still in its infancy in terms of monitoring the
1193 ocean from immediate to climatological timescales.

1194 The relationships between climatological forcing
1195 and biological carbon storage in the ocean are complex

and not readily incorporated in models. Ocean color
imagery can provide assessments of potential changes
to ocean processes including primary productivity,
surface heating, sediment plumes, altered food webs,
harmful algal blooms, changing acidity, and alterations
of benthic habitats in response to shifts in winds and
upwelling, clouds and radiative forcing, and storm
intensity and frequency. Recent observed changes in
chlorophyll, primary production, and the size of the
oligotrophic gyres from ocean color satellites are com-
pelling evidence of significant changes in the global
ocean. A recent study demonstrates that a time series
of at least 40 years in length is needed to unequivocally
distinguish a global warming trend from natural vari-
ability [6] and sustained long-term observations of
ocean color are in jeopardy [40].

In addition to sustained imagery, there is a need for
integrating ocean color imagery from different plat-
forms to monitor the oceans and aquatic habitats at
a variety of desired spectral, spatial, and temporal res-
olutions. Integration of satellite sensors with suborbital
platforms will allow for better assessment of vulnerable
marine and aquatic habitats, as well as responses to
hazards such as harmful algal blooms, oil spills, and
storms that cause coastal flooding and erosion. Active
sensors, such as Light Detection and Ranging (LIDAR),
will allow us to probe into the depths of the oceans.
Moreover, integrating surface ocean color measure-
ments with three-dimensional measurements and
models of the ocean will be increasingly important in
discerning a changing ocean [49].

Finally, the approaches or algorithms for
conducting ocean color remote sensing will be aug-
mented as more spectral channels become routinely
available and as ocean properties change. Purely statisti-
cal or empirical models are only accurate when condi-
tions are similar to past conditions. When
considering a changing ocean, the cause of the color
change must be carefully assessed to separate the spec-
tral variability due to phytoplankton from other
sources of variability, such as sediments, CDOM, and
even atmospheric aerosols. Considerable growth is also
expected in approaches and technology for remote
sensing of coastal habitats and assessing acute and
chronic hazards. Comprehensive and consistent field
observations from ships to autonomous vehicles
and floats are required to assess the accuracy of

1243 satellite-derived products, build improved algorithms,
 1244 and provide better linkages between surface measure-
 1245 ments made from space and the processes within the
 1246 water column [49]. Future effort will also be directed at
 1247 assimilation of ocean color imagery into global circula-
 1248 tion and climate models. As outlined above, remote
 1249 sensing of ocean color is a complex discipline requiring
 1250 radiometrically accurate and calibrated sensors,
 1251 advanced techniques for atmospheric correction of
 1252 aerosols and dust, and approaches that can deduce
 1253 the source of variability in the color signal measured
 1254 by a sensor. With the many important applications of
 1255 ocean color remote sensing, from climate forecasting to
 1256 environmental monitoring, a consistent and coordi-
 1257 nated international investment in education, research,
 1258 and technology is required to maintain and advance
 1259 this dynamic field.

1260 Bibliography

- 1261 1. Carr ME et al (2006) A comparison of global estimates of
 1262 marine primary production from ocean color. *Deep Sea Res*
 1263 *Part II: Top Stud Oceanogr* 53:741–770
- 1264 2. Field CB, Behrenfeld MJ, Randerson JT, Falkowski P (1998)
 1265 Primary production of the biosphere: integrating terrestrial
 1266 and oceanic components. *Science* 281:237–240
- 1267 3. Smith RC, Baker KS (1978) Optical classification of natural
 1268 waters. *Limnol Oceanogr* 23:260–267
- 1269 4. Martinez E, Antoine D, D’Ortenzio F, Gentili B (2009) Climate-
 1270 driven basin-scale decadal oscillations of oceanic phytoplank-
 1271 ton. *Science* 326:1253–1256
- 1272 5. Siegel DA, Franz BA (2010) Century of phytoplankton change.
 1273 *Nature* 466:569–570
- 1274 6. Henson SA et al (2010) Detection of anthropogenic climate
 1275 change in satellite records of ocean chlorophyll and productiv-
 1276 ity. *Biogeosciences* 7:621–640
- 1277 7. IOCCG (2008) Why ocean colour? the societal benefits of
 1278 ocean-colour technology. In: Platt T, Hoepffner N, Stuart V,
 1279 Brown C (eds) *Reports of the International Ocean-Colour Coor-*
 1280 *inating Group*, Dartmouth, Canada
- 1281 8. Morel A (1988) Optical modeling of the upper ocean in rela-
 1282 tion to its biogenous matter content (case I waters). *J Geophys*
 1283 *Res* 93:10749–10768
- 1284 9. Gordon HR, Morel AY (1983) *Remote assessment of ocean*
 1285 *color for interpretation of satellite visible imagery: a review.*
 1286 *Springer*, New York
- 1287 10. O’Reilly JE, Maritorena S, Mitchell BG, Siegel DA (1998) Ocean
 1288 color chlorophyll algorithms for SeaWiFS. *J Geophys Res*
 1289 103:24937–24953
- 1290 11. McClain CR (2009) A decade of satellite ocean color observa-
 1291 tions*. *Annu Rev Mar Sci* 1:19–42
- 1292 12. Kirk JTO (1994) *Light and photosynthesis in aquatic ecosys-*
 1293 *tems.* Cambridge University Press, Cambridge
- 1294 13. Blough NV, Del Vecchio R (2002) Chromophoric DOM in the
 1295 coastal environment. In: Hansell DA, Carlson CA (eds) *Biogeo-*
 1296 *chemistry of marine dissolved organic matter.* Academic, San
 1297 *Diego*, pp 509–546
- 1298 14. Twardowski MS, Boss E, Sullivan JM, Donaghay PL (2004)
 1299 Modeling the spectral shape of absorption by chromophoric
 1300 dissolved organic matter. *Mar Chem* 89:69–88
- 1301 15. Ciotti AM, Cullen JJ, Lewis MR (2002) Assessment of the rela-
 1302 tionships between dominant cell size in natural phytoplank-
 1303 ton communities and the spectral shape of the absorption
 1304 coefficient. *Limnol Oceanogr* 47:404–417
- 1305 16. Bricaud A, Claustre H, Ras J, Oubelkheir K (2004) Natural vari-
 1306 ability of phytoplanktonic absorption in oceanic waters: influ-
 1307 ence of the size structure of algal populations. *J Geophys Res*
 1308 109:C11010
- 1309 17. Stramski D, Boss E, Bogucki D, Voss KJ (2004) The role of
 1310 seawater constituents in light backscattering in the ocean.
 1311 *Prog Oceanogr* 61:27–56
- 1312 18. Mobley CD (1994) *Light and water: radiative transfer in natural*
 1313 *waters.* Academic, San Diego
- 1314 19. Gordon HR et al (2009) Spectra of particulate backscattering in
 1315 natural waters. *Opt Express* 17:16192–16208
- 1316 20. Twardowski MS, Lewis M, Barnard A, Zaneveld JRV (2005) In-
 1317 water instrumentation and platforms for ocean color remote
 1318 sensing applications. In: Miller R, Del-Castillo C, McKeese D (eds)
 1319 *Remote sensing of coastal aquatic waters.* Springer, Dordrecht
- 1320 21. Smith RC, Baker K (1978) The bio-optical state of ocean waters
 1321 and remote sensing. *Limnol Oceanogr* 23:247–259
- 1322 22. Morel A, Gentili B (1993) Diffuse reflectance of oceanic waters.
 1323 II. Bidirectional aspects. *Appl Opt* 32:6864–6879
- 1324 23. Lee ZP, Carder KL, Arnone RA (2002) Deriving inherent optical
 1325 properties from water color: a multiband quasi-analytical algo-
 1326 rithm for optically deep water. *Appl Opt* 41:5755–5772
- 1327 24. Aurin DA, Dierssen HM (2011) Remote sensing requirements
 1328 for the optically complex waters of Long Island Sound. *Remote Sens Environ* (Submitted)
- 1329 25. Ryan JP et al (2005) Coastal ocean physics and red tides: an
 1330 example from Monterey Bay, California. *Oceanography*
 1331 18:246–255
- 1332 26. Mouroulis P, Green RO, Wilson DW (2008) Optical design of
 1333 a coastal ocean imaging spectrometer. *Opt Express*
 1334 16:9087–9096
- 1335 27. Davis CO et al (2002) Ocean PHILLS hyperspectral imager:
 1336 design, characterization, and calibration. *Opt Express*
 1337 10(4):210–221
- 1338 28. McClain CR, Cleave ML, Feldman GC, Gregg WW (1998) Science
 1339 quality SeaWiFS data for global biosphere research. *Sea*
 1340 *Technol* 39:10–16
- 1341 29. Gordon HR (1997) Atmospheric correction of ocean color
 1342 imagery in the Earth Observing System era. *J Geophys Res*
 1343 102:17081–17106
- 1344 30. Antoine D, Morel A (1999) A multiple scattering algorithm for
 1345 atmospheric correction of remotely sensed ocean color
- 1346

- 1347 (MERIS instrument): principle and implementation for atmo-
1348 spheres carrying various aerosols including absorbing ones.
1349 *Int J Remote Sens* 20:1875–1916
- 1350 31. Gao BC, Montes MJ, Ahmad Z, Davis CO (2000) Atmospheric
1351 correction algorithm for hyperspectral remote sensing of
1352 ocean color from space. *Appl Opt* 39:887–896
- 1353 32. Wang M, Son SH, Shi W (2009) Evaluation of MODIS SWIR and
1354 NIR-SWIR atmospheric correction algorithms using SeaBASS
1355 data. *Remote Sens Environ* 113:635–644
- 1356 33. Yan B et al (2002) Pitfalls in atmospheric correction of ocean
1357 color imagery: how should aerosol optical properties be com-
1358 puted? *Appl Opt* 41:412–423
- 1359 34. Fukushima H, Toratani M (1997) Asian dust aerosol: optical
1360 effect on satellite ocean color signal and a scheme of its
1361 correction. *J Geophys Res* 102:17119–17130
- 1362 35. Antoine D, Nobileau D (2006) Recent increase of Saharan dust
1363 transport over the Mediterranean Sea, as revealed from ocean
1364 color satellite (SeaWiFS) observations. *J Geophys Res* 111:
1365 D12214
- 1366 36. Claustre H et al (2002) Is desert dust making oligotrophic
1367 waters greener? *Geophys Res Lett* 29:107–1
- 1368 37. Paytan A et al (2009) Toxicity of atmospheric aerosols on
1369 marine phytoplankton. *Proc Natl Acad Sci* 106:4601
- 1370 38. Garrison VH et al (2003) African and Asian dust: from desert
1371 soils to coral reefs. *Bioscience* 53:469–480
- 1372 39. Monahan EC, O’Muircheartaigh I (1981) Improved statement
1373 of the relationship between surface wind speed and oceanic
1374 whitecap coverage as required for the interpretation of satel-
1375 lite data. In: Gower JFR (ed) *Oceanography from space*. Ple-
1376 num, New York, pp 751–755
- 1377 40. National Research Council Committee on Assessing Require-
1378 ments for Sustained Ocean Color Research and Operations
1379 (2011) *Assessing requirements for sustained ocean color
1380 research and operations*. National Academies Press
- 1381 41. Jerlov NG (1974) *Optical aspects of oceanography*. Academic,
1382 London, pp 77–94
- 1383 42. Morel A, Prieur L (1977) Analysis of variations in ocean color.
1384 *Limnol Oceanogr* 22:709–721
- 1385 43. Mobley CD, Stramski D, Bissett WP, Boss E (2004) Optical
1386 modeling of ocean water: is the case 1 – case 2 classification
1387 still useful? *Oceanography* 17:60–67
- 1388 44. Morel A, Bricaud A (1981) Theoretical results concerning light
1389 absorption in a discrete medium and application to the spe-
1390 cific absorption of phytoplankton. *Deep-Sea Res*
1391 28:1357–1393
- 1392 45. Siegel DA, Maritorena S, Nelson NB, Behrenfeld MJ (2005) Inde-
1393 pendence and interdependencies among global ocean color
1394 properties: reassessing the bio-optical assumption. *J Geophys
1395 Res* 110:C07011
- 1396 46. Swan CM, Siegel DA, Nelson NB, Carlson CA, Nasir E (2009)
1397 Biogeochemical and hydrographic controls on chromophoric
1398 dissolved organic matter distribution in the Pacific Ocean.
1399 *Deep Sea Res Part I: Oceanogr Res Pap* 56:2175–2192
47. Dierssen HM (2010) Benthic ecology from space: optics and
1400 net primary production in seagrass and benthic algae across
1401 the Great Bahama Bank. *Mar Ecol Progress Ser* 411:1–15
1402
48. Zaneveld JRV (1989) An asymptotic closure theory for irradiance
1403 in the sea and its inversion to obtain the inherent optical
1404 properties. *Limnol Oceanogr* 34:1442–1452
1405
49. Dierssen HM (2010) Perspectives on empirical approaches for
1406 ocean color remote sensing of chlorophyll in a changing cli-
1407 mate. *Proc Natl Acad Sci* 107:17073
1408
50. Moore TS, Campbell JW, Dowell MD (2009) A class-based
1409 approach to characterizing and mapping the uncertainty of
1410 the MODIS ocean chlorophyll product. *Remote Sens Environ*
1411 113:2424–2430
1412
51. Schofield O et al (2004) Watercolors in the coastal zone: what
1413 can we see? *Oceanography* 17:25–31
1414
52. Falkowski P et al (2000) The global carbon cycle: a test of our
1415 knowledge of earth as a system. *Science* 290:291
1416
53. Behrenfeld MJ, Falkowski PG (1997) Consumers guide to phy-
1417 toplankton primary productivity models. *Limnol Oceanogr*
1418 42:1479–1491
1419
54. Campbell J et al (2002) Comparison of algorithms for estimat-
1420 ing ocean primary production from surface chlorophyll, tem-
1421 perature, and irradiance. *Glob Biogeochem Cycle* 16:1035
1422
55. Westberry T, Behrenfeld MJ, Siegel DA, Boss E (2008) Carbon-
1423 based primary productivity modeling with vertically resolved
1424 photoacclimation. *Glob Biogeochem Cycle* 22:GB2024
1425
56. Mouw CB, Yoder JA (2005) Primary production calculations in
1426 the Mid-Atlantic Bight, including effects of phytoplankton
1427 community size structure. *Limnol oceanogr* 50(4):1232–1243
1428
57. IOCCG (2006) *Remote sensing of inherent optical properties:
1429 fundamentals, tests of algorithms, and applications*. In: Lee ZP
1430 (ed) *Reports of the International Ocean-Colour Coordinating
1431 Group*, Dartmouth
1432
58. Siegel DA, Maritorena S, Nelson NB, Hansell DA, Lorenzi-Kayser
1433 M (2002) Global distribution and dynamics of colored
1434 dissolved and detrital organic materials. *J Geophys Res*
1435 107:3228
1436
59. U.S. National Aeronautics and Space Administration, Goddard
1437 Earth Sciences, Data and Information Services Center,
1438 *Giovanni*. <http://disc.sci.gsfc.nasa.gov/giovanni/>
1439
60. Behrenfeld MJ et al (2009) Satellite-detected fluorescence
1440 reveals global physiology of ocean phytoplankton.
1441 *Biogeosciences* 6:779–794
1442
61. Dierssen HM, Kudela RM, Ryan JP, Zimmerman RC (2006) Red
1443 and black tides: quantitative analysis of water-leaving radi-
1444 ance and perceived color for phytoplankton, colored
1445 dissolved organic matter, and suspended sediments. *Limnol
1446 oceanogr* 51:2646–2659
1447
62. Brewin RJW et al (2011) An intercomparison of bio-optical
1448 techniques for detecting dominant phytoplankton size class
1449 from satellite remote sensing. *Remote Sens Environ*
1450 115:325–339
1451
63. Balch WM, Kilpatrick KA, Trees CC (1996) The 1991
1452 coccolithophore bloom in the central North Atlantic. 1. Optical
1453

[Au5]

[Au6]

- 1454 properties and factors affecting their distribution. *Limnol*
 1455 *Oceanogr* 41:1669–1683
- 1456 64. Tomlinson MC, Wynne TT, Stumpf RP (2009) An evaluation of
 1457 remote sensing techniques for enhanced detection of the
 1458 toxic dinoflagellate, *Karenia brevis*. *Remote Sens Environ*
 1459 113:598–609
- 1460 65. Simis SGH, Peters SWM, Gons HJ (2005) Remote sensing of the
 1461 cyanobacterial pigment phycocyanin in turbid inland water.
 1462 *Limnol Oceanogr* 50:237–245
- 1463 66. Chavez FP, Ryan J, Lluch-Cota SE, Niqun CM (2003) From
 1464 anchovies to sardines and back: multidecadal change in the
 1465 Pacific Ocean. *Science* 299:217–221
- 1466 67. Platt T, Cesar Fuentes-Yaco KTF (2003) Marine ecology: spring
 1467 algal bloom and larval fish survival. *Nature* 423:398–399
- 1468 68. Fuentes-Yaco C, Koeller PA, Sathyendranath S, Platt T (2007)
 1469 Shrimp (*Pandalus borealis*) growth and timing of the spring
 1470 phytoplankton bloom on the Newfoundland–Labrador Shelf.
 1471 *Fish Oceanogr* 16:116–129
- 1472 69. Seibel BA, Dierssen HM (2003) Cascading trophic impacts of
 1473 reduced biomass in the Ross Sea, Antarctica: just the tip of the
 1474 iceberg? *Biol Bull* 205:93–97
- 1475 70. Rosa R, Dierssen HM, Gonzalez L, Seibel BA (2008) Large-scale
 1476 diversity patterns of cephalopods in the Atlantic open ocean
 1477 and deep sea. *Ecology* 89:3449–3461
- 1478 71. Dekker A et al (2005) Remote sensing of seagrass ecosystems:
 1479 use of spaceborne and airborne sensors. In: Larkum AWD, Orth
 1480 RJ, Duarte CM (eds) *Seagrasses: biology, ecology, and conser-*
 1481 *vation*. Springer, Dordrecht, pp 347–359
- 1482 72. Cavanaugh KC, Siegel DA, Kinlan BP, Reed DC (2010) Scaling
 1483 giant kelp field measurements to regional scales using satellite
 1484 observations. *Mar Ecol Prog Ser* 403:13–27
- 1485 73. Phinn S, Roelfsema C, Dekker A, Brando V, Anstee J (2008)
 1486 Mapping seagrass species, cover and biomass in shallow
 1487 waters: an assessment of satellite multi-spectral and airborne
 1488 hyper-spectral imaging systems in Moreton Bay (Australia).
 1489 *Remote sens Environ* 112:3413–3425
- 1490 74. Lesser MP, Mobley CD (2007) Bathymetry, water optical prop-
 1491 erties, and benthic classification of coral reefs using
 1492 hyperspectral remote sensing imagery. *Coral Reefs*
 1493 26:819–829
- 1494 75. Dierssen HM, Zimmerman RC, Drake LA, Burdige DJ
 1495 (2009) Potential export of unattached benthic macroalgae to
 1496 the deep sea through wind-driven Langmuir circulation.
 1497 *Geophys Res Lett* 36:L04602
- 1498 76. Burdige DJ, Hu X, Zimmerman RC (2008) Shallow water car-
 1499 bonate dissolution and ocean acidification: impacts and
 1500 feedbacks
- 1501 77. Goes JJ, Thoppil PG, Gomes HR, Fasullo JT (2005) Warming of
 1502 the Eurasian landmass is making the Arabian Sea more pro-
 1503 ductive. *Science* 308:545–547
- 1504 78. Beman JM, Arrigo KR, Matson PA (2005) Agricultural runoff
 1505 fuels large phytoplankton blooms in vulnerable areas of the
 1506 ocean. *Nature* 434:211–214
- 1507 79. Dwivedi RM, Solanki HU, Nayak SR, Gulati D, Somvanshi VS
 1508 (2005) Exploration of fishery resources through integration of
 ocean colour with sea surface temperature: Indian experience. *IJMS* 34:430–440
80. Chavez FP, Strutton PG, McPhaden MJ (1998) Biological-
 physical coupling in the Central Equatorial Pacific during the
 onset of the 1997–98 El Niño. *Geophys Res Lett* 25:3543–3546
81. Lewis MR, Platt TC (1987) Remote observation of ocean colour
 for prediction of upper ocean heating rates. *Adv Space Res*
 7:127–130
82. Hill VJ (2008) Impacts of chromophoric dissolved organic
 material on surface ocean heating in the Chukchi Sea. *J Geophys Res* 113:C07024
83. Gnanadesikan A, Anderson WG (2009) Ocean water clarity and
 the ocean general circulation in a coupled climate model. *J Phys Oceanogr* 39:314–332
84. Gnanadesikan A, Emanuel K, Vecchi GA, Anderson WG,
 Hallberg R (2010) How ocean color can steer Pacific tropical
 cyclones. *Geophys Res Lett* 37:L18802
85. Miller WL, Moran MA (1997) Interaction of photochemical and
 microbial processes in the degradation of refractory dissolved
 organic matter from a coastal marine environment. *Limnol*
Oceanogr 42:1317–1324
86. Ackleson SG, Balch WM, Holligan PM (1994) Response of
 water-leaving radiance to particulate calcite and chlorophyll
 a concentrations: a model for Gulf of Maine coccolithophore
 blooms. *J Geophys Res* 99:7483–7499
87. Gordon HR et al (2001) Retrieval of coccolithophore calcite
 concentration from SeaWiFS imagery. *Geophys Res Lett*
 28:1587–1590
88. Balch W, Drapeau D, Bowler B, Booth E (2007) Prediction of
 pelagic calcification rates using satellite measurements. *Deep*
Sea Res Part II: Top Stud Oceanogr 54:478–495
89. Balch WM, Fabry VJ (2008) Ocean acidification: documenting
 its impact on calcifying phytoplankton at basin scales. *Mar*
Ecol Prog Ser 373:239–247
90. Ryther JH (1969) Photosynthesis and fish production in the
 sea. *Science* 166:72–76
91. Wilson RW et al (2009) Contribution of fish to the marine
 inorganic carbon cycle. *Science* 323:359–362
92. Platt T, Sathyendranath S, Fuentes-Yaco C (2007) Biological
 oceanography and fisheries management: perspective after
 10 years. *ICES J Marine Sci* 64:863
93. Platt T, Sathyendranath S (2008) Ecological indicators for the
 pelagic zone of the ocean from remote sensing. *Remote Sens*
Environ 112:3426–3436
94. Stumpf RP et al (2003) Monitoring *Karenia brevis* blooms in
 the Gulf of Mexico using satellite ocean color imagery and
 other data. *Harmful Algae* 2:147–160
95. Hu C et al (2003) MODIS detects oil spills in Lake Maracaibo,
 Venezuela. *Eos AGU Trans* 84:313–319
96. Fingas M, Brown C (2000) A review of the status of advanced
 technologies for the detection of oil in and with ice. *Spill Sci*
Technol Bull 6:295–302
97. Boland RC, Donohue MJ (2003) Marine debris accumulation in
 the nearshore marine habitat of the endangered Hawaiian

Au7

1550 Au8

1563 monk seal, *Monachus schauinslandi* 1999–2001. *Mar Pollut*
 1564 *Bull* 46:1385–1394

1565 98. Donohue MJ, Boland RC, Sramek CM, Antonelis GA (2001) Der-
 1566 elict fishing gear in the Northwestern Hawaiian Islands: diving
 1567 surveys and debris removal in 1999 confirm threat to coral reef
 1568 ecosystems. *Mar Pollut Bull* 42:1301–1312

1569 99. Randolph K et al (2008) Hyperspectral remote sensing of
 1570 cyanobacteria in turbid productive water using optically
 1571 active pigments, chlorophyll a and phycocyanin. *Remote*
 1572 *Sens Environ* 112:4009–4019

1573 100. IOCCG (2007) Ocean-colour data merging In: Gregg W (ed)
 1574 *Reports of the International Ocean-Colour Coordinating*
 1575 *Group*, Dartmouth

1576 **Books and Reviews**

1577 Campbell J, Antoine D, Armstrong R, Arrigo K, Balch W, Barber R,
 1578 Behrenfeld M, Bidigare R, Bishop J, Carr ME et al (2002) Com-
 1579 parison of algorithms for estimating ocean primary produc-
 1580 tion from surface chlorophyll, temperature, and irradiance.
 1581 *Glob Biogeochem Cycle* 16:1035

1582 Carr ME, Friedrichs MAM, Schmeltz M, Noguchi Aita M, Antoine D,
 1583 Arrigo KR, Asanuma I, Aumont O, Barber R, Behrenfeld M et al
 1584 (2006) A comparison of global estimates of marine primary
 1585 production from ocean color. *Deep Sea Res Part II: Top Stud*
 1586 *Oceanogr* 53:741–770

1587 *GlobCOLOUR*: An EO based service supporting global ocean car-
 1588 bon cycle research. European Space Agency. [http://www.](http://www.globcolour.info/)
 1589 [globcolour.info/](http://www.globcolour.info/)

IOCCG. *Reports of the International Ocean-Colour Coordinating* 1590 [Au9]
Group No. 1–10. Dartmouth. [http://www.ioccg.org/](http://www.ioccg.org/reports_ioccg.html) 1591
[reports_ioccg.html](http://www.ioccg.org/reports_ioccg.html) 1592

Jerlov NG, Nielsen ES (eds) (1974) *Optical aspects of oceanography*. 1593
 Academic, London 1594

Miller R, Del-Castillo C, McKee BA (eds) (2005) *Remote sensing of* 1595 [Au10]
coastal aquatic waters. Springer, Dordrecht 1596

Morel A (1991) *Optics of marine particles and marine optics*. In: 1597
 Demers S (ed) *Particle analysis in oceanography*. Springer, 1598
 Berlin, pp 141–188 1599

Morel A, Bricaud A (1986) Inherent optical properties of algal cells 1600
 including picoplankton: theoretical and experimental results. 1601
Can Bull Fish Aquat Sci 214:521–559 1602

National Aeronautics and Space Administration (NASA) *Ocean* 1603
optics protocols for satellite ocean color sensor validation, 1604
 vol I–VI. <http://oceancolor.gsfc.nasa.gov/DOCS/> 1605

National Aeronautics and Space Administration (NASA) *Ocean* 1606
color web. <http://oceancolor.gsfc.nasa.gov/> 1607

Platt T, Nayak S (eds) (2005). Special issue on: ocean colour remote 1608
 sensing. *Indian J Marine Sci* 34(4):341–355 1609

Siegel D (2004) Views of ocean processes from the sea-viewing 1610
 wide field- of-view sensor mission: introduction to the first 1611
 special issue. *Deep Sea Res Part II Top Stud Oceanogr* 1612
 51(1–3):1–3. <http://dx.doi.org/10.1016/j.dsr2.2003.12.001> 1613

The Oceanography Society (2004) Special issue: coastal ocean 1614 [Au11]
 optics and dynamics. *Oceanography* 17(2):32–43 1615

Thomas A, Siegel D, Marra J (2004) Views of ocean processes from 1616
 the sea-viewing wide field- of-view sensor (SeaWiFS) mission: 1617
 introduction to the second special issue. *Deep Sea Res Part II* 1618
Top Stud Oceanogr 51(10–11):911–912. [http://dx.doi.org/](http://dx.doi.org/10.1016/j.dsr2.2004.06.003) 1619
[10.1016/j.dsr2.2004.06.003](http://dx.doi.org/10.1016/j.dsr2.2004.06.003) 1620

Galley Proof

Remote Sensing of Ocean Color. Table 1 Levels of data processing products from ocean color satellites

Level	Processing	Spatial qualities
0	Raw data as measured directly from the spacecraft	Satellite coordinates at highest spatial resolution
1	Converted to radiance using calibrations and sensor characterization information	Satellite coordinates at highest spatial resolution
2	Atmospherically corrected to water-leaving radiance and derived products	Satellite coordinates at highest spatial resolution
3	Derived products have been mapped onto a two-dimensional grid at known spatial resolution and can be averaged over timescales (weekly, monthly)	Regular gridded data at lower spatial resolution (e.g., 4 or 9 km)
4	Products that have been merged or assimilated with data from other sensors, in situ observations, or model outputs	Regular gridded data at lower spatial resolution

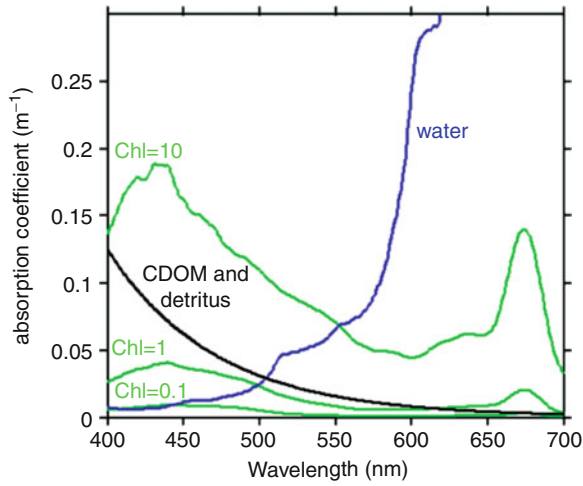
Remote Sensing of Ocean Color. Table 2 Empirical chlorophyll algorithms for a variety of ocean color sensors

Name ^a	Sensor	Channels ^b		Coefficients ^c				
		Blue	Green	a0 ^c	a1	a2	a3	a4
OC4	SeaWiFS	443 > 490 > 510	555	0.366	-3.067	1.93	0.649	-1.532
OC3S	SeaWiFS	443 > 490	555	0.2409	-2.4768	1.5296	0.1061	-1.1077
OC2S	SeaWiFS	490	555	0.2372	-2.4541	1.7114	-0.3399	-2.788
OC3M	MODIS	443 > 488	551	0.283	-2.753	1.457	0.659	-1.403
OC2M	HMODIS	469	555	0.1543	-1.9764	1.0704	-0.2327	-1.1404
OC4O	OCTS	443 > 490 > 520	565	0.4006	-3.1247	3.1041	-1.4179	-0.3654
OC3O	OCTS	443 > 490	565	0.2836	-2.1982	1.0541	0.186	-0.717
OC2O	OCTS	490	565	0.2805	-2.167	1.1789	-0.1597	-1.5591
OC3C	CZCS	443 > 520	550	0.3012	-4.4988	9.0983	-9.9821	3.235

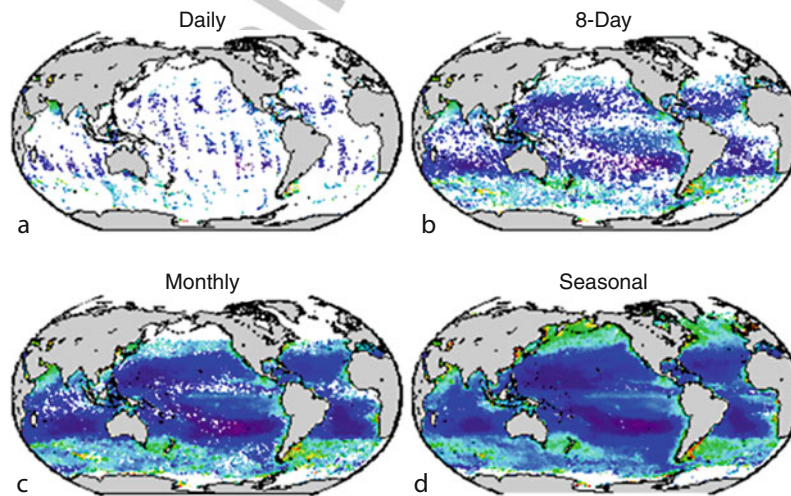
^aName of ocean color (OC) algorithm incorporates the number of wavebands (2–4) used in the formulation and the initial for the sensor used (S = SeaWiFS; M = MODIS; O = OCTS; C = CZCS)

^bThe algorithms use a log-transformed ratio of “Blue” (443–520 nm) to “Green” (550–565 nm) remote sensing reflectance (R_{rs}). When more than one “Blue” channel is provided, only the channel with the highest R_{rs} is used. $x = \log_{10}(R_{rs}(\text{Blue})/R_{rs}(\text{Green}))$

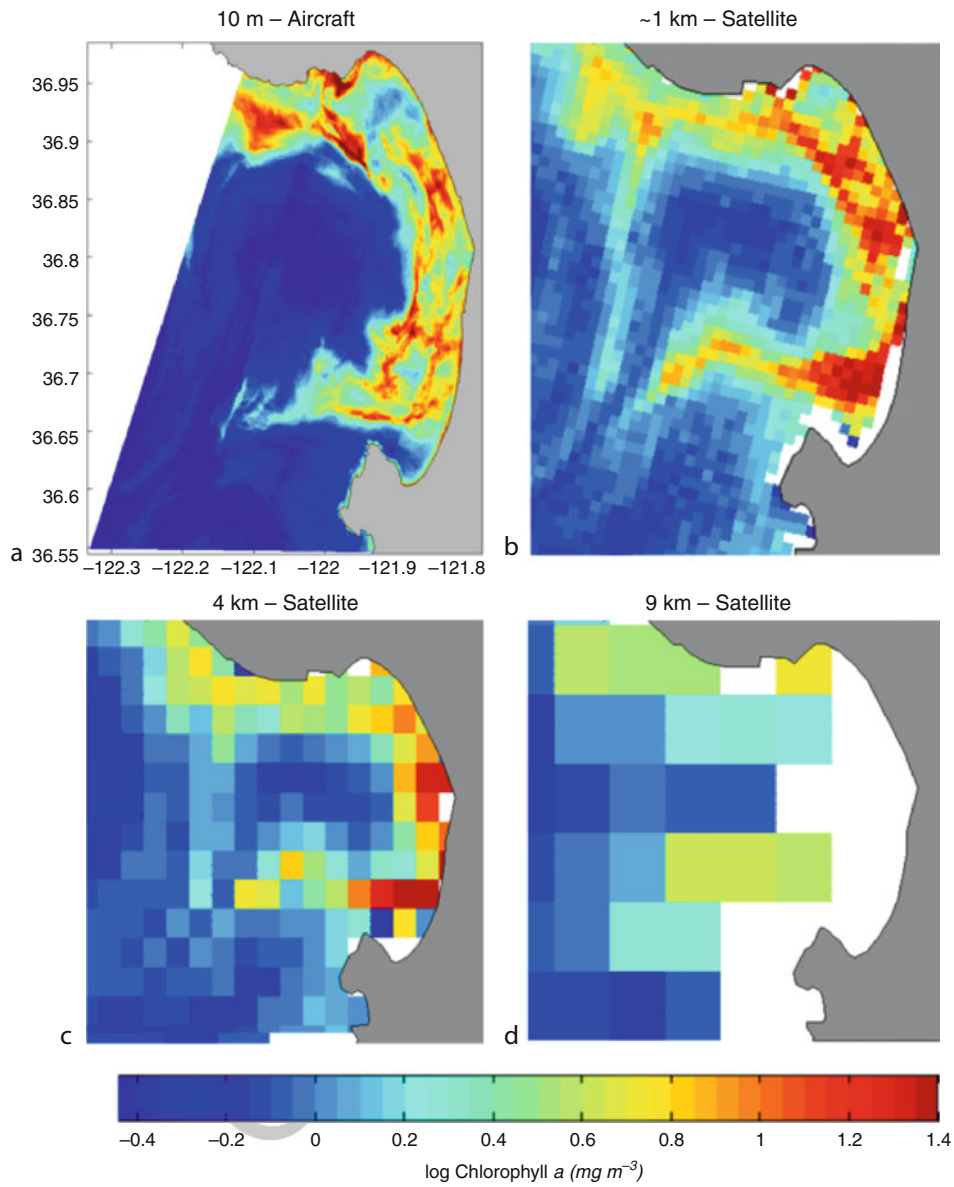
^cChlorophyll a is modeled as a fourth polynomial fit to the field data such that: $\text{Chl} = 10^{(a_0 + a_1 \cdot x + a_2 \cdot x^2 + a_3 \cdot x^3 + a_4 \cdot x^4)}$



Remote Sensing of Ocean Color. Figure 1
Absorption spectrum for different constituents in seawater including water molecules, chromophoric dissolved organic matter and detritus, and phytoplankton contributions bio-optically modeled for chlorophyll ranging from 0.1 to 10 mg m^{-3} [16]

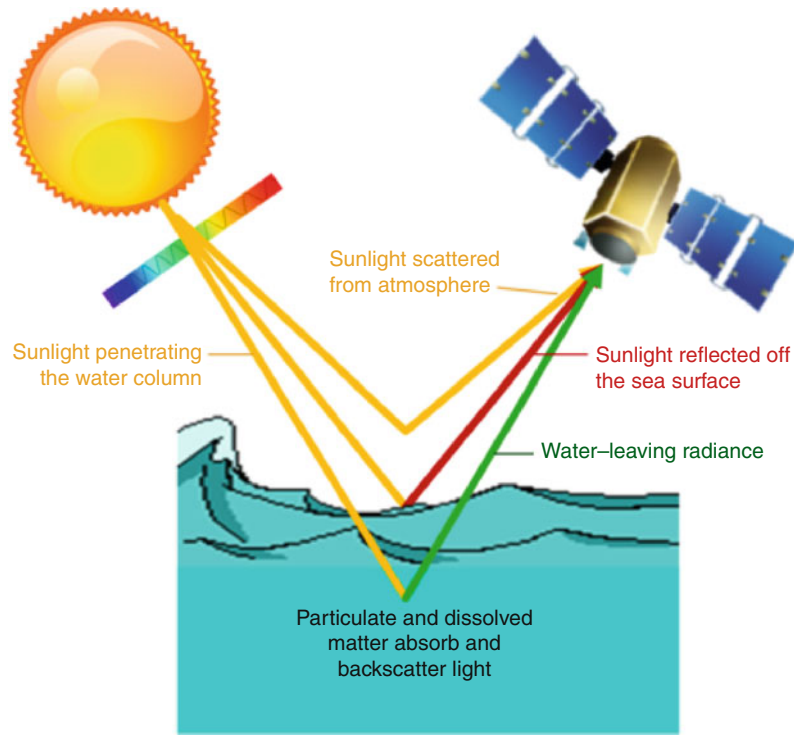


Remote Sensing of Ocean Color. Figure 2
Global maps of satellite-derived chlorophyll showing increasing levels of temporal resolution from daily to seasonal. Imagery from MODIS Aqua satellite from 2006: (a) 17 December; (b) 11–17 December; (c) 1–31 December; (d) Autumn. White spacing in imagery represents gaps in orbital coverage (daily image), as well as clouds and ice cover. Merging of imagery from different sensors can provide enhanced daily coverage [100]



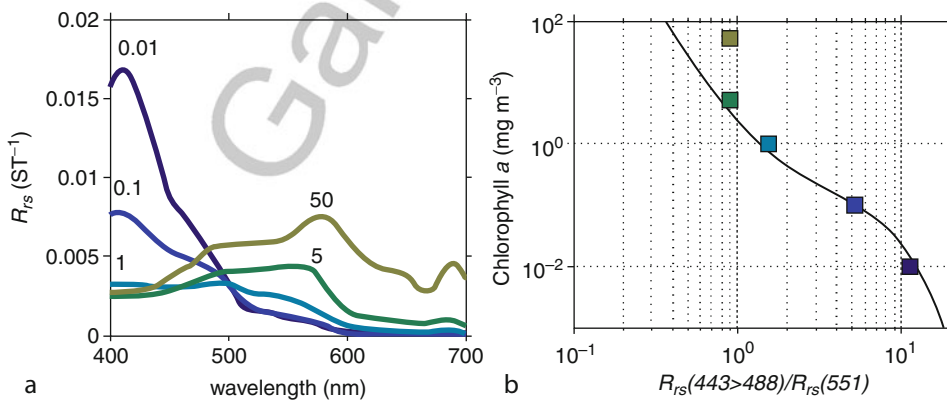
Remote Sensing of Ocean Color. Figure 3

Ocean color remote sensing imagery of Monterey Bay, California, illustrates different spatial resolutions available: (a) AVIRIS sensor flown on an aircraft [25]; (b) SeaWiFS satellite Level 2 data; (c) SeaWiFS satellite gridded to 4-km pixels; (d) SeaWiFS satellite Level 3 9-km standard product



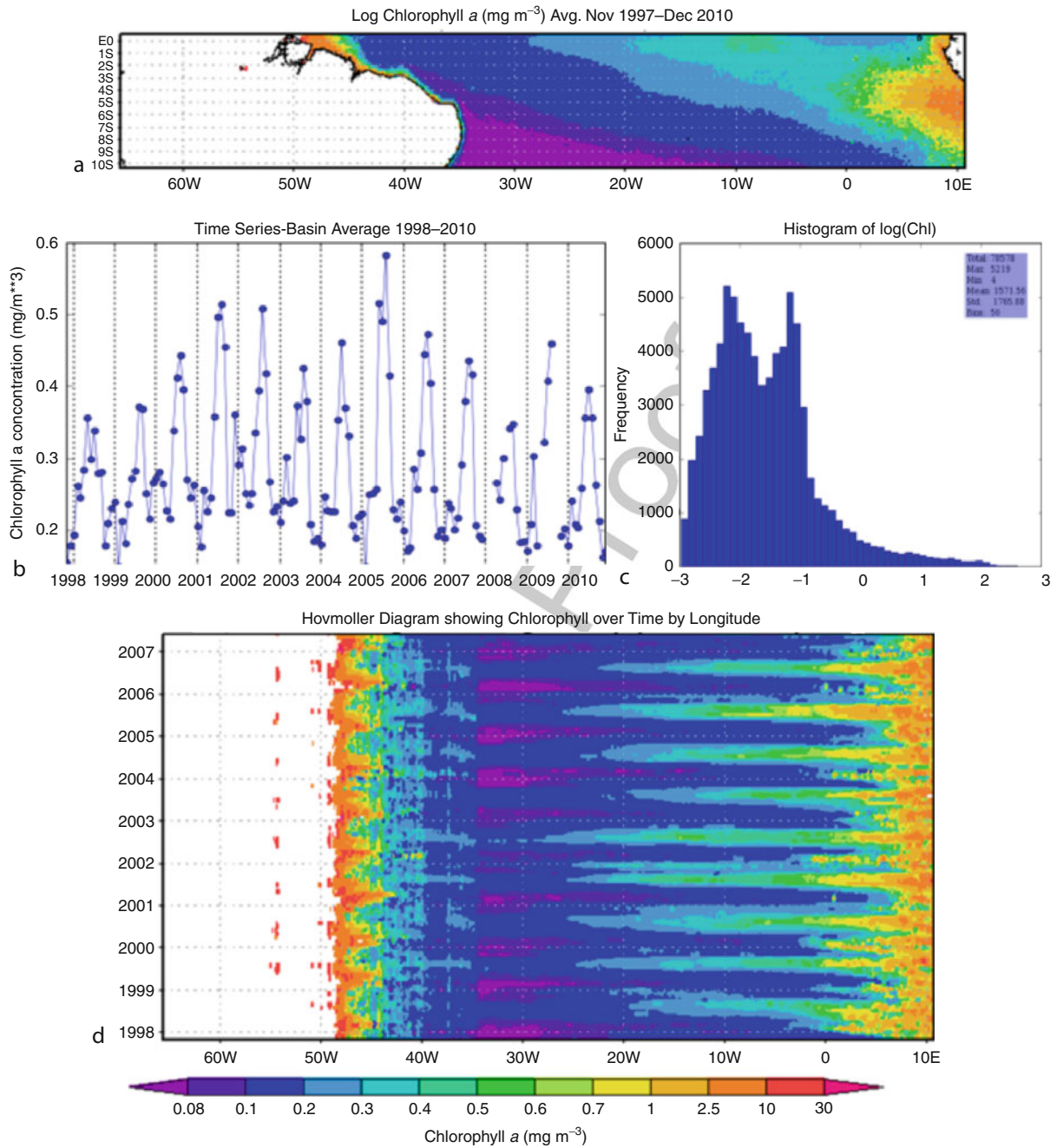
Remote Sensing of Ocean Color. Figure 4

Radiance measured by a satellite includes light scattered by the atmosphere and reflected off the sea surface (i.e., glint). In a process called “atmospheric correction,” these signals are removed leaving the “water-leaving radiance” or the light that has penetrated the water column and been backscattered out to the satellite – a measure of ocean color



Remote Sensing of Ocean Color. Figure 5

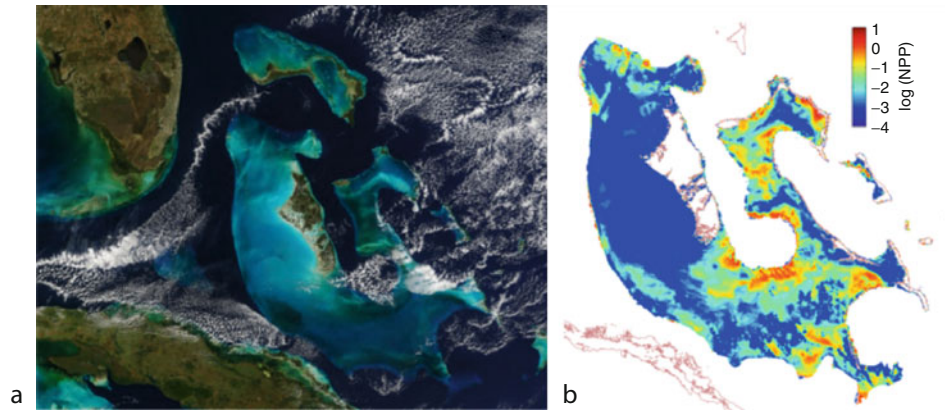
(a) Remote sensing reflectance (R_{rs}) spectra modeled for different concentrations of chlorophyll *a* (Chl) from 0.01 to 50 $mg\ m^{-3}$. The color of each line represents the modeled ocean color a human observer might observe following [61]. (b) The empirical OC3M model for deriving Chl from R_{rs} for the MODIS Aqua sensor. The model uses the “blue” channel with the highest R_{rs} value (443 or 488 nm) divided by the “green” channel at 551 nm. Each square represents the modeled Chl for the corresponding R_{rs} spectra in panel A and demonstrates how the model becomes less accurate at high Chl



Remote Sensing of Ocean Color. Figure 6

Various times series analyses that can be conducted with standard Level 3 chlorophyll imagery including (a) Temporally averaged spatial distributions; (b) time series of interannual variability; (c) histograms showing the statistical distributions; (d) Hovmöller plots presenting both spatial (x-axis) and temporal (y-axis) variability. Such plots can be easily generated by the public with the Giovanni interface [59]

Au12

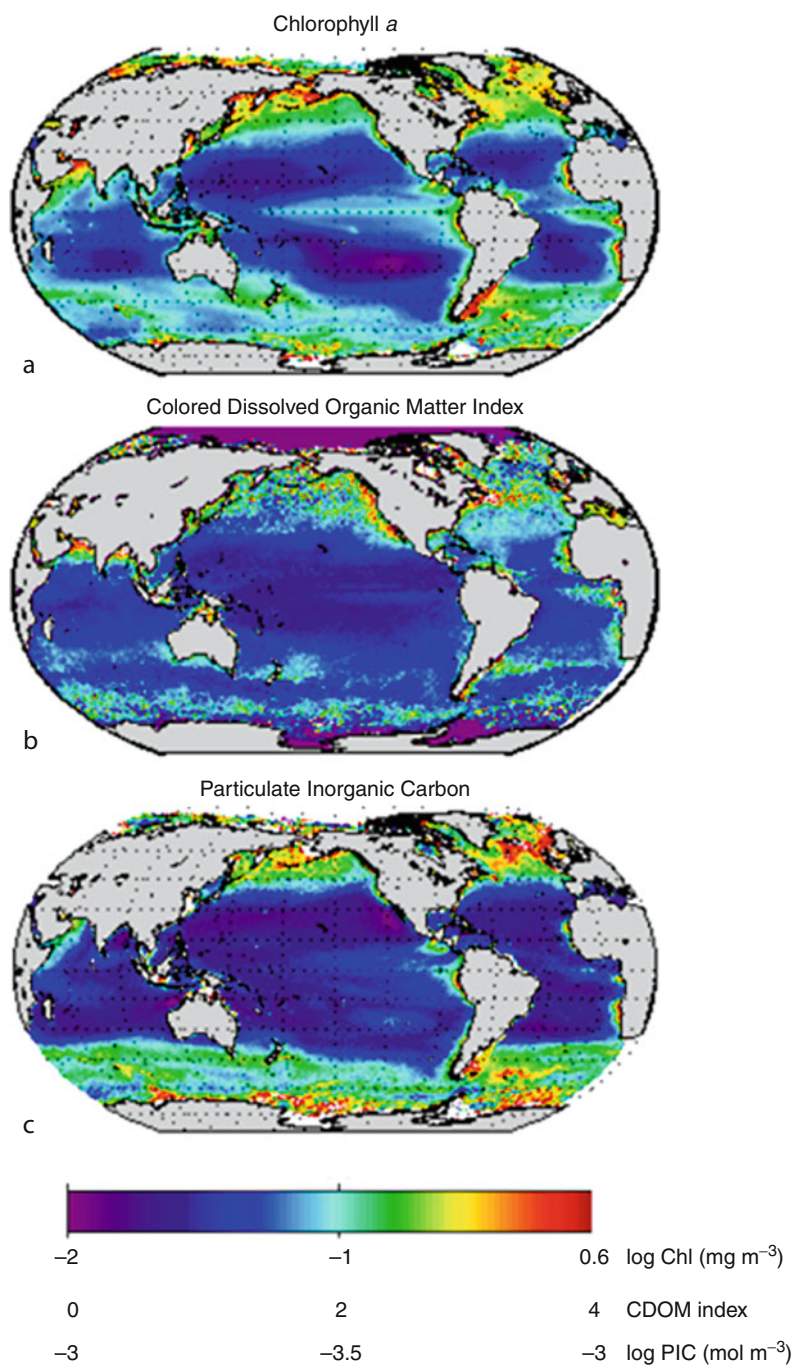


Remote Sensing of Ocean Color. Figure 7

The Great Bahama Bank is an example of optically shallow water where the seafloor color can be observed from space.

(a) Pseudo-true color image from MODIS Aqua showing the bright Bahamas Banks with Florida, USA, to the West and Cuba to the Southwest. White wispy clouds can obscure the ocean color. (b) Net primary productivity ($\text{mgC m}^{-2} \text{d}^{-1}$) of seagrass and benthic algae estimated from ocean color imagery over the Great Bahama Bank [47]

Galley Proof



Remote Sensing of Ocean Color. Figure 8

Global climatologies or long-term averages of products derived from the Ocean Color SeaWiFS sensor from 1998–2011. (a) Chlorophyll *a* (mg m^{-3}); (b) colored dissolved organic matter (CDOM) index; (c) particulate inorganic carbon (PIC) (mol m^{-3})

Author Query Form

Encyclopedia of Sustainability Science and Technology
Chapter No: 737

Query Refs.	Details Required	Author's response
AU1	Kindly provide index terms.	
AU2	Please check if inserted text citation for Table 1 is okay.	
AU3	Variable "a", "Rrs" is found in both roman and italics in the text and in equations. Please confirm which form has to be made consistent.	
AU4	Kindly provide volume and page range for the ref. [24].	
AU5	kindly provide publisher location for the ref. [40].	
AU6	Kindly provide year of publishing for the ref. [59].	
AU7	Kindly provide further details for the ref. [76].	
AU8	Please check if inserted volume number and page range for the Ref. [93] are okay.	
AU9	Kindly provide year of publishing for the references IOCCG, National Aeronautics and Space Administration, Siegel (2004), Thomas et al. (2004), GlobCOLOUR, National Aeronautics and Space Administration.	
AU10	Kindly confirm inserted publisher location in reference Miller et al. (2005).	
AU11	Please check if inserted page range for The Oceanography Society (2004) is okay.	
AU12	Please provide better quality of Fig. 6.	